Quaternary Science Reviews 64 (2013) 121–135

Contents lists available at SciVerse ScienceDirect

Quaternary Science Reviews

journal homepage: www.elsevier.com/locate/quascirev

Paleoglaciation of Shaluli Shan, southeastern Tibetan Plateau

Ping Fu [a,b,*], Arjen P. Stroeven [a], Jonathan M. Harbor [b], Clas Hättestrand [a], Jakob Heyman [b], Marc W. Caffee [c], Liping Zhou [d]

[a] Department of Physical Geography and Quaternary Geology, Stockholm University, Stockholm, SE 10691, Sweden
[b] Department of Earth, Atmospheric, and Planetary Sciences, Purdue University, West Lafayette, IN 47907, USA
[c] Department of Physics, Purdue University, West Lafayette, IN 47907, USA
[d] College of Urban and Environmental Science, Peking University, Beijing 102413, China

ARTICLE INFO

Article history:
Received 3 August 2012
Received in revised form
17 December 2012
Accepted 19 December 2012
Available online

Keywords:
Tibetan Plateau
Glaciation
Cosmogenic exposure dating
Last Glacial Maximum
Monsoon

ABSTRACT

Reconstructing the paleoglaciation of the Tibetan Plateau is critical to understanding linkages between regional climate changes and global climate changes, and here we focus on the glacial history of the Shaluli Shan, an area of the southeastern Tibetan Plateau that receives much of its precipitation from monsoon flow. Based on field investigation, geomorphological mapping, and ^{10}Be exposure dating of moraines, we identify glacial deposits from the Late Glacial, with minimum ages at 13.0 ± 1.2 −17.1 ± 1.6 ka, global Last Glacial Maximum (gLGM) at 21.6 ± 2.0 ka, and pre-gLGM at 102.3 ± 10.0−183.6 ± 17.0 ka. These ages are consistent with and significantly extend the known range from most prior chronological work using terrestrial cosmogenic nuclides in this area, and include a set of dates for the Kuzhaori moraine that raise questions about prior chronologies based on the electron spin resonance technique. Ice caps about 4000 km^2 in size covered the Haizishan Plateau and the Xinlong Plateau during the global LGM, with large glaciers extending far down outlet valleys. The presence of ice cap glaciation, here, contrasts strongly to glaciation elsewhere in the Shaluli Shan and more central regions of the Tibetan Plateau where ice expansion remained constricted to valleys. This work provides important insights into the paleoclimate pattern and monsoon evolution of the Tibetan Plateau over past glacial cycles and indicates that the Shaluli Shan has a glacial chronology more consistent with the Northern Hemisphere paleo-ice sheets than other areas of the Tibetan Plateau.

1. Introduction

The development and chronology of glaciations on the Tibetan Plateau provides valuable information for regional paleoclimate reconstruction and understanding the dynamics of global environmental change and the role of the Plateau in global climate systems (Molnar and England, 1990; Raymo and Ruddiman, 1992; Owen et al., 2002, 2005; Harris, 2006). Moreover, because glaciers can be powerful agents of bedrock erosion, which in turn can impact rates of uplift, constraining glacial timing is important in quantifying the impacts of glaciation on alpine landscape evolution and in evaluating the role of glacial erosion in climate change and tectonics (Hallet et al., 1996; Fabel and Harbor, 1999; Montgomery, 2002; Delmas et al., 2009; Owen, 2009; Owen et al., 2009a). The timing and extent of glaciations on the Tibetan Plateau has been the subject of extensive debate, as summarized in Derbyshire et al. (1991) and Owen (2009), with many unanswered questions remaining because of limited geomorphological mapping and inadequate age control.

Early efforts to constrain the chronology of late Quaternary glaciations on the Tibetan Plateau used relative age dating, radiocarbon techniques and, more recently, luminescence and electron spin resonance (ESR) dating (Richards, 2000; Yi et al., 2007). However, the application of these methods has been hindered by limited availability of some sample materials as well as limitations of some of the techniques when applied to glacial deposits. Application of terrestrial cosmogenic nuclide (TCN) exposure dating in recent decades has significantly refined our understanding of glacial chronologies on the Tibetan Plateau by providing apparent exposure ages for glacial landforms and eroded bedrock (Phillips et al., 2000; Schäfer et al., 2002; Owen et al., 2003, 2005, 2009b; Abramowski et al., 2006; Koppes et al., 2008; Kong et al., 2009; Seong et al., 2009; Dortch et al., 2010; Heyman et al., 2011b). Reviews by Owen (2009) and Owen et al. (2008) show that glacier expansion on the Tibetan Plateau occurred during the Holocene, marine oxygen isotope stage (MIS) 2 and MIS 3, but that these

* Corresponding author. Department of Physical Geography and Quaternary Geology, Stockholm University, Stockholm, SE 10691, Sweden. Tel.: +46 8164728; fax: +46 8164818.
E-mail address: ping.fu@natgeo.su.se (P. Fu).

0277-3791/$ – see front matter © 2013 Elsevier Ltd. All rights reserved.
http://dx.doi.org/10.1016/j.quascirev.2012.12.009

events vary in timing and extent across the Plateau. In areas on the southeastern Tibetan Plateau affected by the southwest Asian monsoon, more extensive glacial advances occurred during MIS 3 than the global Last Glacial Maximum (gLGM), while in the northwestern Tibetan Plateau there was a more extensive advance during gLGM, indicating better correspondence to Northern Hemisphere ice sheet fluctuations in areas dominated by the westerlies (Phillips et al., 2000; Richards et al., 2000; Seong et al., 2007). A thorough compilation of TCN data from the Tibetan Plateau by Heyman et al. (2011a) shows that individual glacial boulder ages on the Tibetan Plateau range from 0.09 ± 0.05 ka to 561.7 ± 54.8 ka. There is a paucity of data older than 20 ka, probably because of a poor preservation of landforms from pre-LGM glaciations. However, the bulk of the TCN exposure ages are from the west, the Himalayas and mountains along the Qinghai-Tibet highway, and few dates are from the vast but largely inaccessible interior region and limited age control for the old glaciations in the margin of the Tibetan Plateau. Furthermore, the varying age results and the chronological uncertainties hamper efforts to compare and correlate glacial timing across the Tibetan Plateau. Thus there is a strong need for studies in areas lacking dating results but with an abundance of glacial landform features to better allow for a correlation between regions of the Tibetan Plateau and with records of glaciations elsewhere.

Another controversial issue is the relationship between the uplift of the Tibetan Plateau and the timing and extent of glaciations. Whereas many Chinese researchers argue that uplift has a strong influence on the timing and extent of glaciations in this region (Shi et al., 1986, 2006; Zheng and Wang, 1996; Zheng and Rutter, 1998; Shi, 2002; Zheng et al., 2002; Liu et al., 2006), most studies of Quaternary glaciations on the Tibetan Plateau do not explicitly consider uplift as an external driving factor. Based on field observations of glacial deposits in the Himalaya, and using relative age relationships, Chinese scholars proposed a much constricted Xixiabangma glaciation during the early Pleistocene, an extensive Nieniexiongla glacial stage during the middle-Pleistocene induced by intense uplift, and penultimate, LGM, and Holocene glaciations of intermediate extent (Shi et al., 1986, 2006). This has been the framework used by Chinese scholars in interpreting glacial deposits across the Plateau, and as the basis for correlating glacial deposits between regions. For instance, in the Shaluli Shan (Shan = mountain range) study area, a ridge in the Kuzhaori valley has been interpreted as a glacial deposit formed during an event named locally the Daocheng glaciation which has been correlated with the most extensive glaciation (Zheng and Ma, 1995; Xu and Zhou, 2009) and is therefore considered of middle-Pleistocene age. The authors similarly argue that intense uplift of the Tibetan Plateau during the middle-Pleistocene triggered maximum glaciations in this area. They also argue that continued uplift during the Pleistocene increased mountain elevations surrounding the Shaluli Shan area, creating a rain shadow as monsoon flow precipitation was intercepted, leading to smaller late Pleistocene glaciations.

Because the Shaluli Shan region displays an abundance of glacial landforms (Fu et al., 2012) yet is an area where firm age constraints are scarce, and because we consider the concept of cross-plateau correlations of glacial stages without absolute age constraints to be unreliable, we here investigate the glacial chronology of the southeastern Tibetan Plateau centered on Shaluli Shan (Fig. 1). To assess the timing of glaciations we present 55 ^{10}Be exposure ages which we combine with geomorphological mapping (Fu et al., 2012) to develop a paleoglaciological reconstruction of the Shaluli Shan.

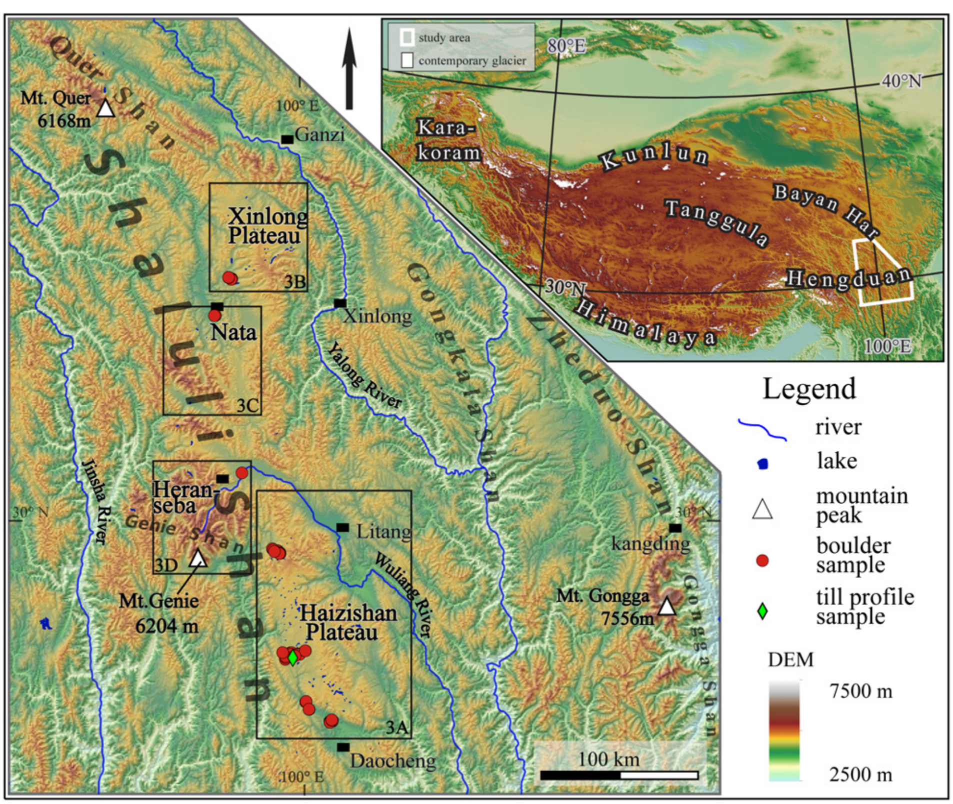

Fig. 1. Location and topographic map of the Shaluli Shan area. Locations of Fig. 3A, B, C, and D are indicated with black rectangles. DEM from Jarvis et al. (2008), lake polygons from United States Geological Survey (http://www.usgs.gov), rivers from National Geomatics Center of China (http://ngcc.sbsm.gov.cn/english/about.asp), and contemporary glaciers for the inset are from GLIMS (http://www.glims.org).

2. Study area and previous studies

The study area is located in the eastern part of the Hengduan Mountains. This area was among the most extensively glaciated areas on the Tibetan Plateau during the Quaternary (Li et al., 1991). The study area is close to the margin of the southeastern Tibetan Plateau, and includes the Shaluli Shan and a series of other NW-SE trending mountain ranges (Fig. 1). The topography of the Shaluli Shan is characterized by high-relief mountains, with deeply incised valleys, and two low-relief plateau uplands, the Haizishan Plateau and the Xinlong Plateau. Plateau-elevations are primarily between 3500 and 4800 m above sea level (asl), with the highest mountain peaking at 7556 m asl (Mt. Gongga). The climate is characterized by the summer monsoon system which accounts for more than 90% of the 300–1000 mm of annual precipitation (Zheng, 2006). Abundant glacial landforms indicate the presence of extensive Quaternary glaciations, although there are few contemporary glaciers in the area, and these occur almost exclusively in the high mountains of the Gongga Shan, Genie Shan and Quer Shan.

Previous studies of the glacial geomorphology and sedimentology of Shaluli Shan have generally outlined the existence of regional ice caps and extensive valley glaciers during two old glaciations during the middle-Pleistocene and the last glaciation and constricted alpine glacier extents during the Holocene (Li et al., 1991; Zheng and Ma, 1995; Zheng, 2001). Chronological constraints on the timing of the youngest two glaciations of the Shaluli Shan have mainly come from radiocarbon, thermoluminescence and ESR dating techniques (Zheng and Ma, 1995; Lehmkuhl et al., 1998; Zheng, 2000, 2001, 2006; Xu and Zhou, 2009). TCN techniques have been applied more widely across the Tibetan Plateau only during the past decade. Several studies have provided TCN exposure and optically stimulated luminescence ages that have begun to provide a chronological framework for the LGM and Holocene glaciations in the Shaluli Shan and Gongga Shan (Schäfer et al., 2002; Owen et al., 2005; Zhou et al., 2007; Graf et al., 2008; Strasky et al., 2009).

In one valley off the Haizishan Plateau, the Kuzhaori valley (close to Daocheng, Fig. 1), an outlet glacier built a moraine complex that was dated using ESR by Xu and Zhou (2009). They suggested that the moraine complex (16.2–134.2 ka) and a highly-weathered outer ridge remnant (556.7 ka) correlated with glaciations at gLGM, early MIS 2, MIS 3, MIS 6 and MIS 14/12. About 1 km to the east of the moraine complex, the outer remnant ridge was dated by Wang et al. (2006) to 100.6–146.5 ka (boulder) and 298.3 ka (limiting surface exposure age derived from a till profile) using ^{10}Be exposure age dating. On neighboring Xinlong Plateau (Fig. 1), Graf et al. (2008) identified a late glacial event (14.9–15.6 ka), a glacial advance at gLGM (17.5–21.6 ka) and an older glaciation with a minimum age of ~43 ka based on boulder ^{10}Be exposure ages. Close to Heranseba (Fig. 1), Schäfer et al. (2002) dated a retracted moraine deposited by a valley glacier to 16.2 ka. Xu et al. (2010) provided OSL and ESR ages from two moraines in a valley of the Quer Shan (Fig. 1) interpreted as a more extensive glaciation at MIS 3 and a restricted glacial advance at MIS 2. Owen et al. (2005) dated two Holocene moraines (^{10}Be exposure age spreads of 0.31–2.42 ka and 7.57–9.51 ka) on Gongga Shan. To the north of Mt. Gongga, near Kangding, Strasky et al. (2009) used erratic boulder ^{10}Be and ^{21}Ne exposure ages to date a glacial advance at the time of Heinrich 1 cooling (13.4–16.3 ka). Zhou et al. (2007) identified two glacial stages around MIS 6 and MIS 2 based on moraine boulder ^{10}Be exposure ages spreads of 112.9–136.5 ka and 11.1–18.5 ka, respectively, in the Boduizangbu River valley in the middle section of the Hengduan Mountains.

3. Methods

3.1. Sampling strategy

We collected 52 samples from glacial boulders to constrain the glacial chronology of the Shaluli Shan using ^{10}Be exposure dating (Figs. 2–4). The samples can be subdivided into four groups based on their locations; Haizishan Plateau, Xinlong Plateau, Nata and Heranseba. On the Haizishan Plateau, Fu et al. (2012, 2013) mapped clearly visible moraine sequences that provided evidence for multiple glaciations and reported field observations of dispersed erratic boulders outside the mapped moraine limits. These dispersed boulders, together with samples from the Xinlong Plateau, Nata and Heranseba, were collected to date the oldest glaciations, and thus samples were taken primarily from glacial traces furthest distanced from the ice accumulation areas. Most samples were from granite boulders on moraines and some from erratic boulders that were dispersed across the landscape. In addition to the 52 samples from boulders we collected 3 till samples from a till profile. The till profile is located in an ice marginal moraine on the Haizishan Plateau, at a location where we sampled four boulders from its surface.

We sampled 1–5 cm thick layers from the top surface of large boulders. For most sample groups, three or four boulders were sampled. We measured topographic shielding using a compass and clinometer, and boulder dimensions and location coordinates were recorded. Photographs were taken for each sample for future reference (Fig. 2). The till profile samples consist of pebbles that were collected at 20 cm, 83 cm, and 202 cm below the surface. The apparent exposure ages of the three profile samples were interpolated and extrapolated toward the surface to calculate a surface exposure age (Owen et al., 2006; Heyman et al., 2011b). The purpose of sampling both four boulders on the surface of a moraine and three samples from a natural cut in the same moraine is to test the consistency of the two methods for surface exposure dating,

Fig. 2. Examples of photographs of boulders sampled for ^{10}Be surface exposure age dating. Sample TB-09-03 is from Nata (group Q in Fig. 3C), TB-09-14 from the Haizishan Plateau surface (group J in Fig. 4C), TB-09-120 from the Kuzhaori moraine off the southern Haizishan Plateau margin (group B in Fig. 4A).

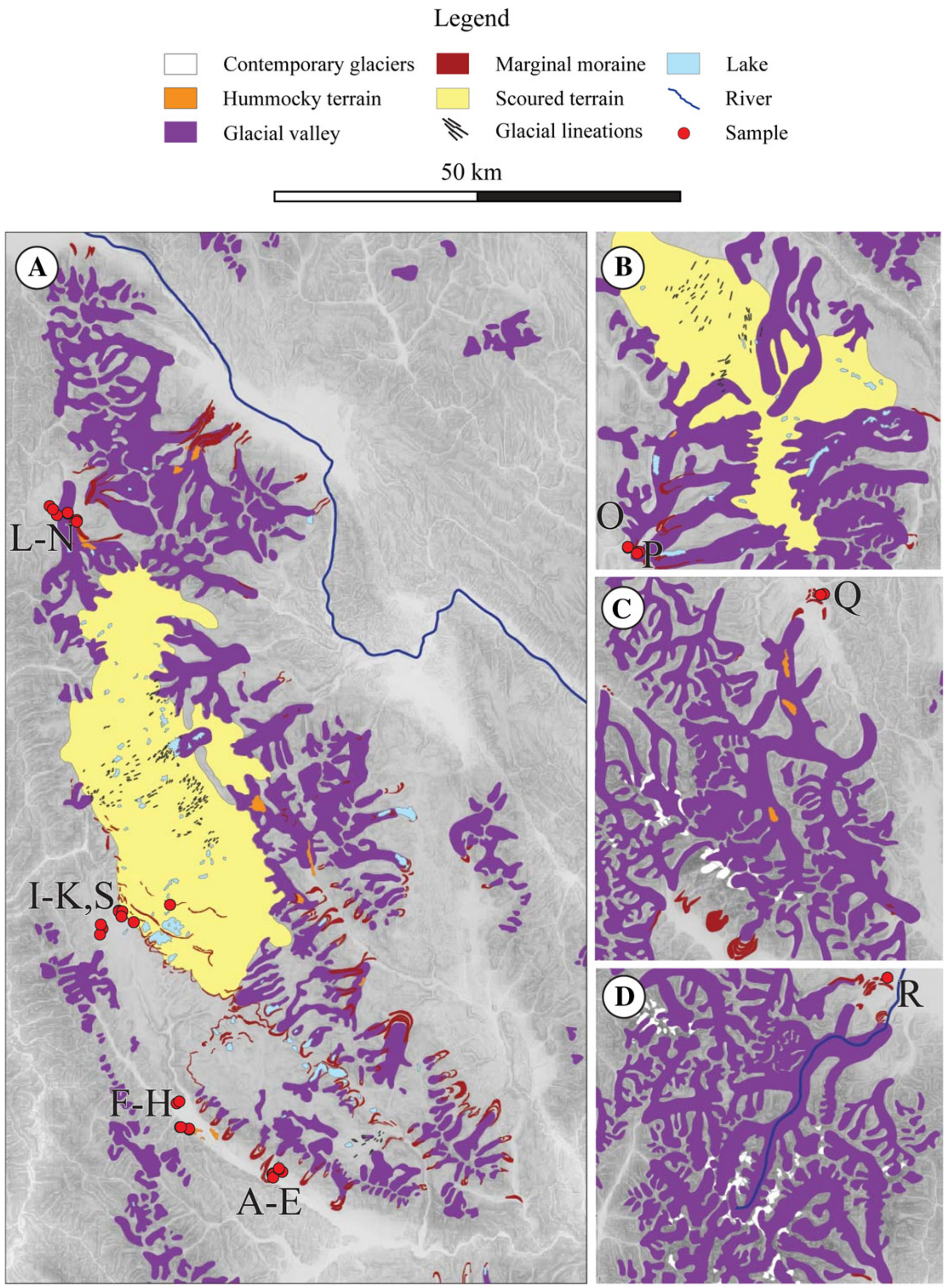

Fig. 3. Glacial landforms and sample locations (red dots) at the four study sites considered. (A) Haizishan Plateau, (B) Xinlong plateau, (C) Nata, and (D) Heranseba. Group name of samples are labeled as black letters (cf Table 1) and larger-scale images of the sample groups from panel a are given in Fig. 4. Mapped landforms are from Fu et al. (2012). Panel locations are given in Fig. 1. (For interpretation of the references to color in this figure legend, the reader is referred to the web version of this article.)

given that different samples (surface-depth, boulders-pebbles) may have different exposure histories (e.g., Heyman et al., 2011b).

3.2. Laboratory methods

Rock samples were crushed and sieved to 250–500 μm at Peking University. Geochemistry for quartz separation was performed at the Purdue Rare Isotope Measurement Laboratory (PRIME Lab) and included procedures modified from Kohl and Nishiizumi (1992), ^{9}Be addition, and beryllium purification and oxidation. Ratios of ^{10}Be/^{9}Be were measured by accelerator mass spectrometry (AMS) at PRIME Lab and calibrated using the ICN ^{10}Be standard with the revised ^{10}Be/^{9}Be ratio (Nishiizumi et al., 2007). The ratios were converted to ^{10}Be concentrations using sample weights and total beryllium. Apparent exposure ages were calculated using the CRONUS online calculator (version 2.2; Balco et al., 2008) with a ^{10}Be

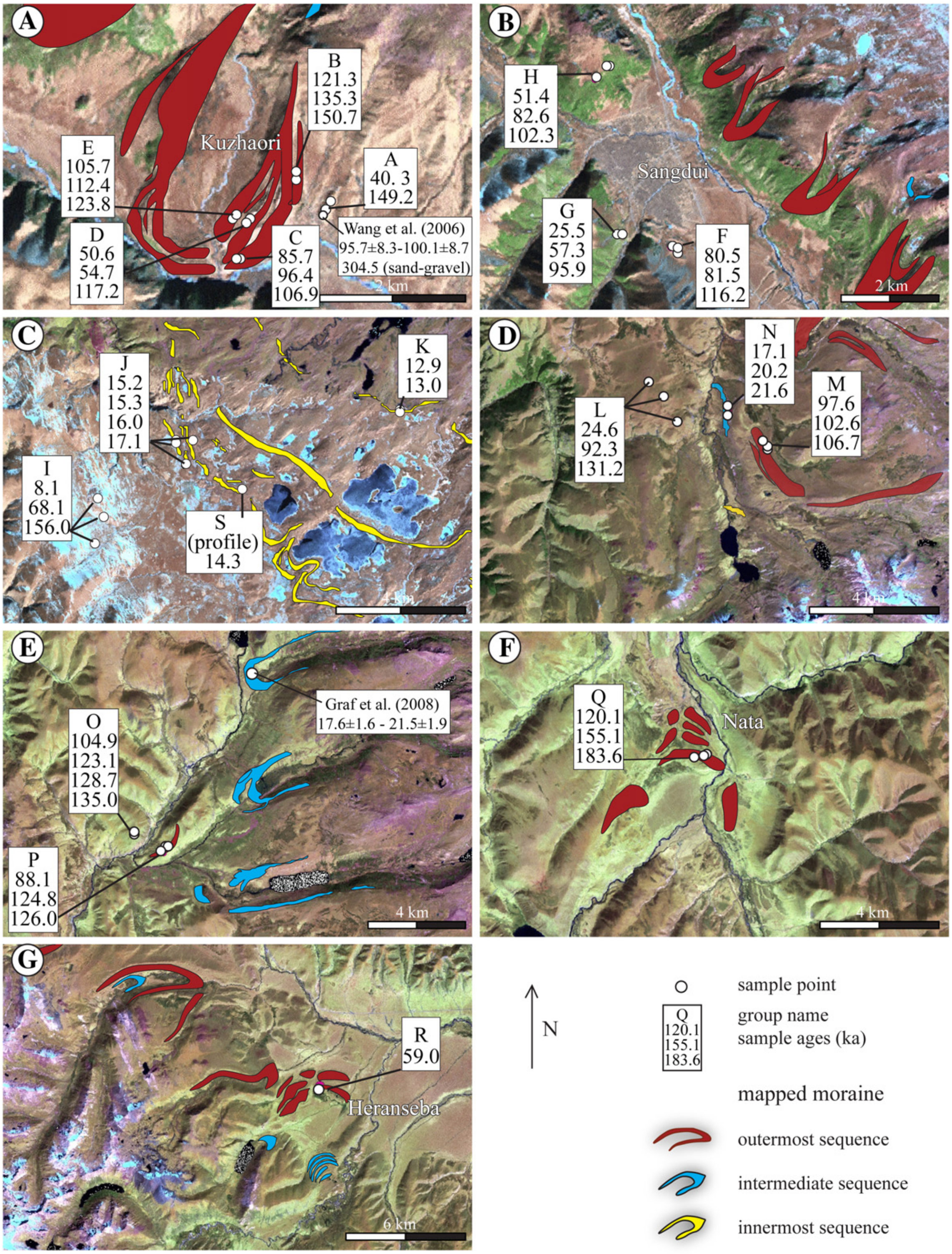

Fig. 4. Sample ages labeled on satellite images with mapped ice marginal moraine features. (A) Kuzhaori, (B) Sangdui, (C) Haizishan Plateau surface, (D) northern Haizishan plateau, (E) Xinlong plateau, (F) Nata, (G) Heranseba. The three moraine sequences are colored by their morphostratigraphical position. While the innermost and intermediate moraines in different areas can be correlated to the same glaciations, the outermost moraine have highly variable exposure ages. In panels A and E, ages from previous studies are recalculated from the original nuclide concentrations using CRONUS with the corresponding ^{10}Be standardization and time-dependent Lal (1991)/Stone (2000) scheme.

half-life of 1.387 Ma (Chmeleff et al., 2010; Korschinek et al., 2010) and the revised ^{10}Be standardization (Nishiizumi et al., 2007). Exposure ages are presented under the assumptions of zero post-depositional surface erosion and rock density of 2.7 g/cm^3. CRONUS age uncertainties are composed of two parts, where internal methodological uncertainties due to AMS measurements are the same for all scaling schemes, but where external uncertainties vary with production rate scaling schemes (Balco et al., 2008).

The principle behind interpolating the till profile data to derive a surface exposure age is that the nuclide concentration (N_z) at any depth in a sediment section with no post-depositional disturbance is a function of depth (z) and surface nuclide concentration (N_0) (Nishiizumi et al., 1989):

$$N_Z = N_0{*}\exp(-\rho z/\Lambda) \tag{1}$$

where ρ is till density and Λ is the cosmic ray attenuation length (160 g/cm^2; Gosse and Phillips, 2001; Balco et al., 2008). For a till section with a uniform density, N_z of samples at different depths should fit perfectly on an exponential curve in N_z–z space. Using the Nelder and Mead (1965) simplex method, constants N_0 and ρ can therefore be derived from concentrations at depth. For a till section in a moraine with constant density, the surface nuclide concentration extrapolated from the samples at depth should be close to the nuclide concentration in boulder surfaces sampled from the same moraine. Previous studies (Owen et al., 2006; Wang et al., 2006; Heyman et al., 2011b) have arrived at till densities of 1.8 g/cm^3 in the Kuzhaori valley, 2.02 g/cm^3 in the Ladakh Range, Himalaya, and 1.6 or 1.8 g/cm^3 in the Bayan Har Shan, northeastern Tibetan Plateau. Although this method works well in some locations, sediments in a given section might have been disturbed by cryoturbation or may have been derived from different sources with different prior exposure histories, and thus may not fit the ideal exponential curve.

4. Site descriptions

4.1. Haizishan Plateau

The Haizishan Plateau is a low-relief granite pluton, located primarily above 4000 m asl, which is surrounded by sedimentary rocks. An elongated bedrock ridge protrudes 100–300 m above the central plateau surface, but is asymmetrically located near the eastern edge of the plateau, resulting in a broad flat area to the west and high-relief terrain on the east (Fu et al., 2013). The plateau is topographically separated from neighboring mountainous terrain by tectonic basins and fluvial valleys. Detailed geomorphological studies of the plateau by Fu et al. (2012, 2013) provide evidence for an extensive ice cap and outlet glaciers complex, and a zonation of glacial landforms indicating the ice cap had polythermal basal ice conditions (Fig. 3). The asymmetric topography of the plateau forced the paleo-ice cap to form asymmetric landform patterns (Fig. 3). Whereas a broad area of scoured terrain west of the central ridge is bordered by a relatively narrow zone of glacial valleys, on the east side there is only a narrow zone of scoured terrain that transitions rapidly into a deeply cut and broad zone of glacial valleys without cirque heads.

Geomorphological mapping and field investigations reveal the presence of multiple moraine sequences, indicating past glacial stages of varying extent (Fu et al., 2012, 2013; Fig. 3). The most distinct and widespread sets of moraines or moraine complexes are located most distal to former glaciation centers, and are imprints of the terminus of outlet glaciers or ice cap margins. These moraine complexes often include two to five ridges which, in places like the Kuzhaori valley, are overlapping (Fig. 4A). The outermost ridge in the Kuzhaori moraine complex (B in Fig. 4A), appears to be more weathered and has fewer boulders than the inner four ridges (C–E in Fig. 4A), and the frontal part of the outermost ridge is missing and was either removed by post-depositional fluvial or glacial erosion or was buried by deposits of younger glaciation(s). Within 1 km to the east of the moraine complex (A in Fig. 4A), a ridge with deeply weathered sediments could be a moraine remnant that belongs to a much older glacial stage than the overlapping four moraines, as was suggested by Xu and Zhou (2009) who inferred an ESR-dated formation age of 556.7 ka. A second and much less distinctive moraine sequence occurs a few kilometers headwards in valleys on the west side of the plateau but much closer to the valley mouth on the eastern side. These moraines were first mapped in detail by Fu et al. (2012), and many of them have been reworked by fluvial processes leaving only remnant terminal sections or lateral moraines. The third, highest, and innermost moraine sequence includes up to three, over 20 km-long, distinctly sinuous moraine ridges on the western scoured terrain unit of the Haizishan Plateau (Figs. 3A and 4C) and remnant ridges in the valleys on its east side. During field investigations dispersed boulders and moraine remnants were observed to occur well beyond the outermost moraine sequences, indicating that still more extensive glaciations occurred than indicated by glacial geomorphology alone. These major events have never been identified previously.

We sampled at four main locations to determine if chronologies were consistent across the Haizishan Plateau. The four locations are the Kuzhaori valley in the southwest (Figs. 3A and 4A), Sangdui valley in the west (Figs. 3A and 4B), the plateau surface (Figs. 3A and 4C), and a valley in the northern part (Figs. 3A and 4D). In Kuzhaori valley, samples were collected from the moraine remnant (group A, two samples) and 4 moraines (groups B, C, D, and E) were sampled of the moraine complex. In Sangdui valley (Fig. 4B), three groups of samples were collected, one from a lateral moraine on the nose of an interfluve just north of Sangdui village (group H), the other two from dispersed boulders on ridges west of Sangdui village (groups G and F). Two of the three sinuous moraines on the plateau surface, except the intermediate one, were sampled (groups J, K; Fig. 4B). In addition, three erratic boulders (group I) were sampled about 10 km beyond and west of the outermost sinuous moraine and three till profile samples were collected from the outermost sinuous moraine (group S). In a valley draining the northern part of the Haizishan Plateau (Fig. 4D), we sampled the frontal part of a lateral moraine close to the valley bottom (group N) and a large but degraded lateral moraine ridge (group M) located on a platform on the east valley side. Three dispersed granite boulders on schist bedrock were collected from rounded hills on the west side of the valley (group L). In total, 15 groups of boulder samples were collected from the Haizishan Plateau and, except for groups A and K, each contains three or four samples.

4.2. Xinlong Plateau

The Xinlong Plateau is located 200 km north of the Haizishan Plateau (Fig. 1) and consists of a low-relief granite core (4400–4600 m asl) and bedrock ridge (4600–4900 m asl) extending N–S from the southern part of the plateau (Fig. 3B). Deeply cut glacial valleys without cirque heads extend from the southern bedrock ridge while the larger plateau surface to its north is characterized by scoured terrain (Fu et al., 2012; Fig. 3B). The glacial lineations and scoured terrain together with the outlet glacial valleys indicate the former presence of an ice cap or ice field (Fu et al., 2013). The clearest moraine complex in this area visible on remote sensing imagery consists of five or six end moraine ridges at a valley mouth with lateral moraines extending several kilometers up the valley (Fig. 3B). There is a moraine remnant mapped on a bedrock ridge several kilometers further down the valley, and two additional end moraines were identified from field inspection along the valley. Graf et al. (2008) presented TCN ages ranging from 17.5 ka to 21.6 ka for boulder samples from the moraine complex at the valley mouth, from 14.9 ka to 15.6 ka from the inner two end moraines and 35.1 ka and 48.2 ka for two perched boulders close to the central highland. They interpreted the three features as representing a Late Glacial advance responding to the Heinrich 1 event (Heinrich, 1988), a glacial advance during MIS 2 synchronous to gLGM, and an older glaciation, respectively. Beyond the dated moraine at the valley mouth, we sampled three boulders (group P) from a moraine ridge remnant on a bedrock crest between two valleys, and four erratics (group O) on top of a hill which is about 100 m higher than the moraine (Fig. 3B).

4.3. Nata

The Nata region has one of the most spectacular alpine landscapes in the Shaluli Shan area, and its largest glacial valley is about 45 km long (Fig. 3C). The highest summit peaks at 5812 m asl, and the range is separated from the mountainous area to its south by a valley 3 to 4 km wide with its floor at 4000–4100 m asl. The north side of the range is only 20–30 km wide, with elevations decreasing to 4000 m asl. Glacial valleys in the northern region are much longer than those in the southern region. Glaciers formed distinct moraine complexes in valleys on the southern side, similar to the Kuzhaori moraine complex off the southern margin of Haizishan Plateau. On the northern side, on the other hand, there is a notable absence of comparable moraine complexes. Field investigations have revealed that moraine remnants on the northern side are exceptionally wide (about 500–700 m in width), and have gentle slopes and a small number of dispersed boulders on their surfaces. A large flat area reflecting fluvial or glaciofluvial deposition is located between these moraine remnants and the glacial valley mouth. Rivers have eroded the moraine and deposited distinct terraces that extend downvalley from the moraines. We collected three boulder samples (group Q) from the top of the innermost moraine.

4.4. Heranseba

The Heranseba area hosts a spectacular alpine landscape, with Mt. Genie peaking at 6204 m asl (Fig. 3D). Glacial valleys up to 30 km long radiate from the central peak. The longest valley is situated on the northern side and hosts a moraine complex consisting of several ridges at its mouth. Several moraine remnants are situated on a broad flat plain 3 km beyond this moraine complex. The landscape of Heranseba is similar to that of Nata, with a similar occurrence of outer moraine remnant ridges. One sample from such a moraine remnant was dated (group R).

5. Results

Apparent exposure ages for all samples were calculated using the information listed in Table 1. The samples are grouped into 18 boulder groups (A-R) and 1 till profile group (S). The apparent exposure ages range from 8.1 ± 0.8 ka to 183.6 ± 17.0 ka (Table 1, Fig. 4). The apparent exposure ages of the landforms generally conform well to their morphostratigraphical positions, except for those on the inner three moraines of the Kuzhaori valley (groups C, D and E).

6. Discussion

6.1. Age spreads

Large age spreads can be observed within each group (Fig. 5A). Significant age spreads such as observed in the Shaluli Shan constitute one of the biggest challenges in interpreting ^{10}Be results (Hallet and Putkonen, 1994; Putkonen and Swanson, 2003; Briner et al., 2005; Owen et al., 2005, 2006, 2008, 2009b; Putkonen and O'Neal, 2006; Putkonen et al., 2008; Applegate et al., 2010, 2012; Heyman et al., 2011b). There are two major geological factors affecting the age spread from any given set of boulders from one location (or landform), incomplete exposure and prior exposure. Incomplete exposure includes the processes of weathering, exhumation, and shielding of the surface by snow or sediment. All these processes may individually or jointly reduce nuclide concentrations in rock or sediments, compared to a full postglacial exposure history of the samples, thereby underestimating the true age of deposition/deglaciation. Prior exposure, or inheritance, increases the nuclide concentration beyond a full postglacial exposure history and thereby overestimates the true age of deposition. The importance of these two factors was assessed by Heyman et al. (2011a) based on a large collection of TCN ages from boulders in glaciated areas from around the world. They concluded that incomplete exposure is more important than prior exposure because (i) only 4% of boulders used to date northern hemisphere paleo-ice sheet positions had ages that differed more than ten thousand years from reconstructed ages of local deglaciation based on other reliable dating methods, and (ii) none of the recently deposited boulders transported by contemporaneous glaciers had exposure ages significantly deviating from independently known depositional ages. Furthermore, Heyman et al. (2011a) show that within-group age spreads are predictable using a degradation model, whereas a prior exposure model fails to predict the observed boulder age distributions. The results of this analysis reaffirm the importance of collecting multiple samples from depositional surfaces such as moraines. If ages of multiple boulders in a group are similar, the implication is that of insignificance of degradation or prior exposure. However, where age spreads within a boulder group occur, which is commonly the case, the spread is probably caused by post-depositional exhumation or weathering processes. In this case it would be correct to accept the oldest apparent exposure age in a boulder group to represent the best estimate of the minimum age of deposition/deglaciation. For the Shaluli Shan, the largest age spreads occur in two groups of boulders (I and L) collected from formerly glaciated surfaces beyond distinct mapped moraines. One possible interpretation is that each of the boulders may have originated from different glaciations. Another possible interpretation is that they all relate to the same glaciation, albeit with different exhumation ages from till, which was removed by fluvial erosion.

Adopting the oldest age of each sample group, three major clusters of moraine boulder samples can be recognized (Fig. 5B): a youngest cluster with exposure ages ranging from 13.0 ± 1.2 ka (TB-09-112) to 17.1 ± 1.6 ka (TB-09-13), an intermediate cluster at 21.6 ± 2.0 ka (TB-09-76), and an oldest cluster ranging from 102.3 ± 10.0 ka (TB-08-01) to 183.6 ± 17.0 ka (TB-09-03).

The ages presented here are calculated using the time-dependent production rate model of Lal (1991)/Stone (2000), which has been widely adopted in calculating ^{10}Be exposure ages for glacial chronology (Balco, 2011). Large variations in exposure ages can result from the application of different scaling models, especially in low-latitude and high-altitude locations such as on the Tibetan Plateau (Owen et al., 2009b; Balco, 2011). To test the robustness of our derived exposure ages using one production rate model, we recalculated all the ages for our samples, located at 29–31° N and 3800–4600 m asl, using three other widely adopted time-varing models (Dunai, 2001; Lifton et al., 2005; Desilets et al., 2006) and a time-constant Lal (1991)/Stone (2000) model. Predictably, the variations that result from using these alternative production rate models are much larger for older apparent exposure ages than younger ones. For example, recalculations of the oldest exposure age (TB-09-03, 183.6 ± 17.0 ka) yielded a variation from −14% to 20% when compared to the time-dependent Lal (1991)/Stone (2000) age. The implication is that by using the time-constant Lal (1991)/Stone (2000) production rate model, the timing of the oldest recorded glacial event in the area would shift from at least MIS 6 back to at least MIS 7 (220 ka). Derived variations for the youngest apparent exposure ages, in contrast, only range from −8%

Table 1
Apparent exposure ages and CRONUS inputs of samples.

Location[a]	Sample group[b]	Sample name	Latitude (°N)	Longitude (°E)	Elevation (m asl)	Sample thickness (cm)	Boulder size length*width *height (m)	^{10}Be concentration (atoms/g)	uncertainty in ^{10}Be concentration (atoms/g)	Exposure age with external uncertainty (ka)[c]	Internal uncertainty (ka)
HZS - KZR	A	TB-08-18	29.12553	100.22237	3892	2	2.4*1.7*0.5	7827647	164708	149.2 ± 13.5	4.0
	A	TB-08-10	29.12415	100.22163	3871	1	3.5*1.7*2	2084297	65233	40.3 ± 3.7	1.5
	B	TB-09-120	29.12907	100.21812	3924	2	6*5*1.6	8012489	262649	150.7 ± 14.2	6.3
	B	TB-09-121	29.12948	100.21820	3929	4	3*1.5*2	7176619	295393	135.3 ± 13.1	7.1
	B	TB-09-119	29.12847	100.21805	3919	3	6*4*2.5	6479634	133499	121.3 ± 10.8	3.2
	C	TB-08-32	29.11882	100.20948	3864	2		5534562	120464	106.9 ± 9.6	2.9
	C	TB-08-33	29.11893	100.20963	3864	2		4915283	102300	96.4 ± 8.6	2.4
	C	TB-08-34	29.11897	100.20985	3867	2		4360926	126357	85.7 ± 7.8	3.0
	D	TB-08-22	29.12288	100.21147	3916	3	5*4*3.5	6230089	194946	117.2 ± 10.9	4.6
	D	TB-08-23	29.12342	100.21185	3928	3	5*3*1.5	2877747	105209	54.7 ± 5.1	2.4
	D	TB-08-24	29.12360	100.21198	3931	3	4*2*1.5	2700506	84991	50.6 ± 4.6	1.9
	E	TB-08-21	29.12258	100.20882	3904	4	1.5*1*1	6513632	238263	123.8 ± 11.7	5.8
	E	TB-08-20	29.12295	100.20913	3904	5	2*1.5*2	5812484	147660	112.4 ± 10.2	3.6
	E	TB-08-19	29.12353	100.20957	3904	2	6*3*3	5571308	97268	105.7 ± 9.3	2.3
HZS-SD	F	TB-08-28	29.17543	100.10657	4053	1	3*3*2	6745227	166465	116.2 ± 10.5	3.6
	F	TB-08-26	29.17457	100.10770	4067	3	0.9*0.9*0.3	4563242	297350	81.5 ± 8.9	6.4
	F	TB-08-27	29.17530	100.10678	4056	2	1.6*0.7*0.4	4523014	191634	80.5 ± 7.7	4.1
	G	TB-08-29	29.17771	100.09525	4062	3	2.5*2*0.8	5294601	135234	95.9 ± 8.7	3.0
	G	TB-08-30	29.17765	100.09519	4062	2	2.3*1.7*0.8	3191645	95884	57.3 ± 5.2	2.0
	G	TB-08-31	29.17777	100.09523	4064	1.5	3*2*0.8	1334108	37865	25.5 ± 2.3	0.8
	H	TB-08-01	29.20672	100.09058	4216	3	7*5*3	6247289	274133	102.3 ± 10.0	5.5
	H	TB-08-02	29.20897	100.09300	4215	3		4980105	190271	82.6 ± 7.8	3.8
	H	TB-08-03	29.20897	100.09300	4231	3	5*4*2.5	3192983	121110	51.4 ± 4.8	2.4
HZS-PS	I	TB-09-101	29.39737	99.99385	4499	3	2*1.6*0.8	11011911	246145	156.0 ± 14.1	4.5
	I	TB-09-102	29.40253	99.99217	4512	4	2.9*2.2*0.9	4741402	111113	68.1 ± 6.1	1.9
	I	TB-09-100	29.39033	99.99083	4506	4.5	5*4*3	496252	18903	8.1 ± 0.8	0.3
	J	TB-09-13	29.41885	100.01755	4431	2	2*1*0.6	1047811	34925	17.1 ± 1.6	0.6
	J	TB-09-12	29.41848	100.01782	4424	2	7*5*4	968473	33026	16.0 ±1.5	0.6
	J	TB-09-14	29.41877	100.02230	4446	5	11.5*7*5	900914	34603	15.2 ± 1.4	0.6
	J	TB-09-15	29.41178	100.02077	4424	4.5	6.6*6.2*6.8	901018	35488	15.3 ± 1.4	0.6
	K	TB-09-112	29.42658	100.08858	4461	3	5.5*3*2.5	785493	33737	13.0 ± 1.2	0.6
	K	TB-09-114	29.42657	100.08890	4459	4	2*2*1.6	772488	27307	12.9 ± 1.2	0.5
HZS-NP	L	TB-09-130	29.85378	99.93718	4440	3	2*1*1.6	9213369	197387	131.2 ± 11.8	3.6
	L	TB-09-129	29.86075	99.93195	4485	3.5	3.3*2.3*0.7	6380809	168216	92.3 ± 8.3	2.9
	L	TB-09-128	29.86533	99.92715	4504	2	0.9*0.8*0.3	1626225	57542	24.6 ± 2.3	0.9
	M	TB-09-78	29.84657	99.96537	4450	3	6*4*2	7421466	269125	106.7 ± 10.1	4.8
	M	TB-09-77	29.84760	99.96508	4444	5	12.5*8*1.5	6964769	245159	102.6 ± 9.6	4.4
	M	TB-09-79	29.84610	99.96567	4455	4	2.5*2.5*1.1	6664799	115631	97.6 ± 8.6	2.1
	N	TB-09-76	29.85655	99.95317	4311	4	4*2.2*2.5	1260059	46121	21.6 ± 2.0	0.8
	N	TB-09-75	29.85673	99.95308	4313	3	3*2*1.9	1184282	33861	20.2 ± 1.8	0.6
	N	TB-09-74	29.85743	99.95310	4339	4	4*3.3*1.7	992215	39244	17.1 ± 1.6	0.7
XL	O	TB-09-62	31.03130	99.70825	4371	3	4.5*3.5*1.9	9387503	184244	135.0 ± 12.1	3.3
	O	TB-09-63	31.03112	99.70820	4369	3	3*2*0.7	8947551	208913	128.7 ± 11.6	3.8
	O	TB-09-65	31.03225	99.70828	4373	2	1.6*1.5*1	8647890	190875	123.1 ± 11.1	3.4
	O	TB-09-64	31.03253	99.70820	4379	5	4*2.5*1.3	7104294	218367	104.9 ± 9.7	3.9
	P	TB-09-57	31.02600	99.72370	4250	4	1.8*1.7*1	8192745	204919	126.0 ±11.4	4.0
	P	TB-09-56	31.02635	99.72408	4258	3	6*5*1.8	8212087	182648	124.8 ± 11.2	3.5
	P	TB-09-58	31.02390	99.72135	4233	3	5.4*3.2*0.8	5551872	131718	88.1± 7.9	2.5
NT	Q	TB-09-03	30.86843	99.64295	4036	3	3.6*3*0.6	10472668	272273	183.6 ± 17.0	6.0
	Q	TB-09-02	30.86815	99.64302	4043	3	5*3.3*1.1	8984509	256643	155.1 ± 14.4	5.6
	Q	TB-09-04	30.86763	99.63770	4063	3	*1.3*1.2*0.5*	7124691	114697	120.1 ± 10.6	2.4
HR	R	TB-09-20	30.18708	99.77310	4241	3	3*2*1	3671694	109843	59.0 ± 5.4	2.1
HZS-PS	S	TB-09-106	29.40483	100.03797	4465	202[d]		165878	7090		
	S	TB-09-107	29.40483	100.03797	4465	83[d]		445238	16211		
	S	TB-09-108	29.40483	100.03797	4465	20[d]		2698202	81805		
	S	*surface*	*29.40483*	*100.03797*	*4465*	*0*		*887046*		14.3 ± 1.2[e]	

[a] Abbreviations are as follows: HZS-KZR: Kuzhaori valley of the Haizishan Plateau; HZS-SD: Sangdui near the Haizishan Plateau; HZS-PS: Haizishan Plateau surface; HZS-NP: Northern part of Haizishan Plateau; XL: Xinlong Plateau; NT: Nata; HR: Heranseba.
[b] Sample group names for each location reflect their morphostratigraphical order; they are ordered from older to younger.
[c] The apparent exposure ages derive from the time-varying production rate model of Lal (1991)/Stone (2000) calculated using CRONUS online calculator version 2.2 (Balco et al., 2008). They are furthermore based on a ^{10}Be half-life of 1.387 Ma (Chmeleff, 2010; Korschinek et al., 2010) and the revised ICN ^{10}Be standard by Nishiizumi et al. (2007), 07KNSTD.
[d] Sample depth below surface.
[e] The exposure age is calculated from the surface ^{10}Be concentration, an extrapolated value derived from the bottom two till samples at depth, with an assumed till density of 1.3 g/cm^3.

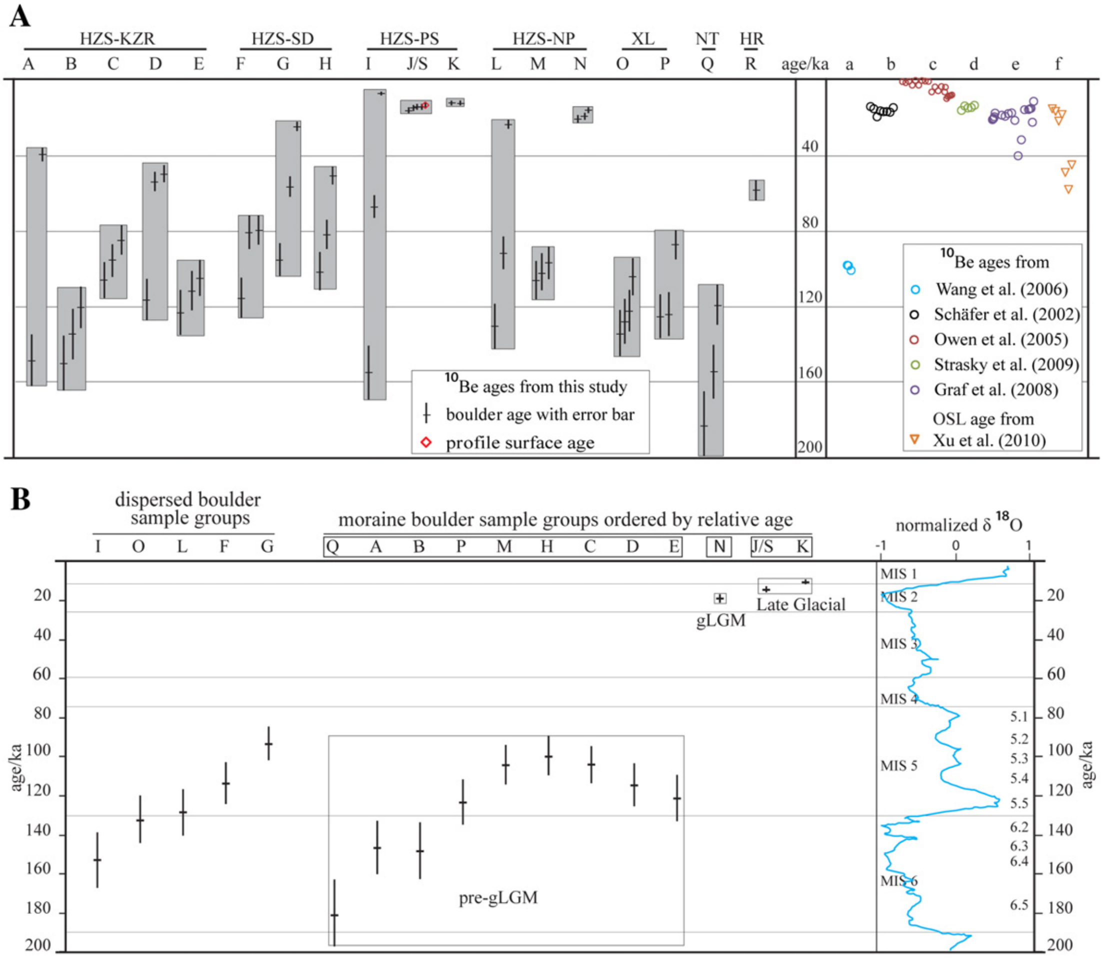

Fig. 5. Plots of ^{10}Be ages. (A), Plot of boulder ages and till profile interpolated age. Age data in the right column are from previous studies in the Shaluli Shan area. Ages from references are recalculated from the original nuclide concentrations using CRONUS with the corresponding ^{10}Be standardization and time-dependent Lal (1991)/Stone (2000) scheme. (B), plot of the oldest age in each group. Group R of Heranseba is not included because interpretation of moraine minimum age based on only one boulder age results in higher uncertainty than on multiple boulder ages because of the large age spread within each sample group. The right column is the standard chronology for marine oxygen isotope records, adapted after Bradley (2001). The rectangles group together samples that overlap each other and do not overlap samples in other rectangles; they also represent the three major glaciations in the Shaluli Shan.

to 5%. For example, the apparent exposure age of TB-09-76 (21.6 ± 2.0 ka), could at most yield an exposure age of 23 ka, which would be the same age within uncertainty. Hence, in this case, using other production rate models would still yield results that are consistent with the maximum stage of MIS 2 glaciation.

6.2. Erosion-corrected exposure ages

Table 1 presents exposure ages assuming zero surface erosion. However, field observations of weathering on some of the sampled boulders show that this assumption is not necessarily valid. Estimating surface erosion rates is difficult in most locations, however, Wang et al. (2006) describe a site near the outermost sinuous moraine on the Haizishan Plateau where this has been possible. They found that the bedrock surface beneath a large erratic was 9 cm higher than the surrounding exposed bedrock surface and they estimated from this height difference, and the exposure age of the surrounding surface, a bedrock erosion rate of 6.9×10^{-5} cm/yr. Assuming steady state erosion, we used the CRONUS calculator to derive a maximum erosion rate of nearly 3.2×10^{-4} cm/yr for our oldest sample (TB-09-03), which is a reasonable estimate of weathering for granitic rocks in alpine environments (Ivy-Ochs et al., 2006). Using erosion rate values representing low and high erosion scenarios of 1×10^{-5} cm/yr and 3×10^{-4} cm/yr, respectively, we recalculated the exposure ages for samples TB-09-03 (183.6 ka), TB-08-01 (102.3 ka), TB-09-76 (21.6 ka), TB-09-13 (17.1 ka), and TB-09-112 (13.0 ka), which are the end members of the three clusters observed in Fig. 5B. The erosion-correction increases the apparent exposure ages by 20%–230% for TB-09-03, 10%–40% for TB-08-01, 2%–5% for TB-09-76, 1%–4% for TB-09-13, and 1%–3% for TB-09-112. Thus neglecting surface weathering and erosion results in large underestimates of exposure ages of older samples but has little impact on exposure ages of relatively young boulders. Because of large uncertainties in erosion estimates, and difficulties to constrain erosion rates for individual boulders, the discussion below is based on minimum apparent exposure ages assuming zero erosion as presented in Table 1.

6.3. Till profile

An exponential regression fit was used to derive an apparent surface exposure age for the till section (Group S, Table 1, Figs. 4c, 6). Using all three samples, the extrapolated concentration at the till surface, N_0, of 4.7×10^6 atoms/g, is much higher than the average boulder nuclide concentration at nearby location J (Table 1; 9.5×10^5 atoms/g; an average concentration is used here because

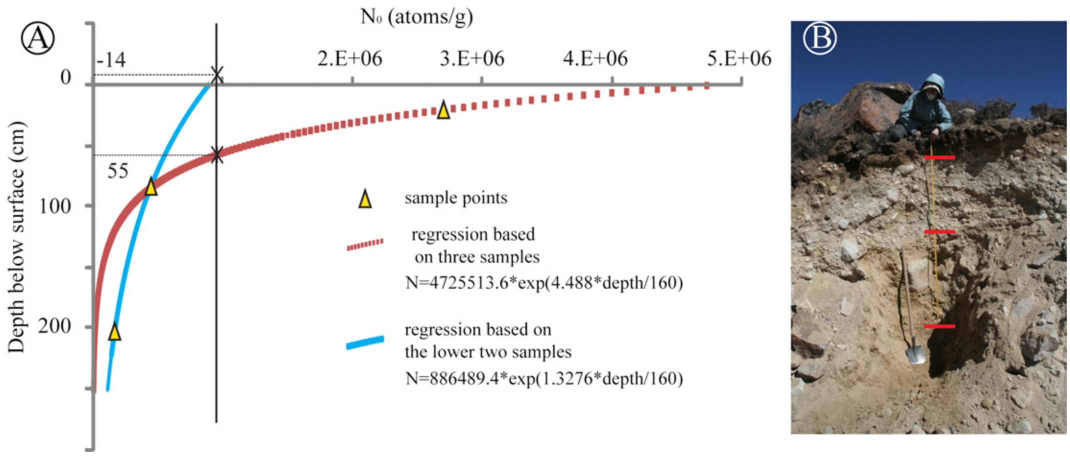

Fig. 6. Interpolation of till profile samples and sample photo. (A) Till section sample regressions. The exponential curves are derived from fitting Equation (1) to the measured ^{10}Be concentrations and uncertainties using software SciDAVis and adopting the Nelder and Mead (1965) simplex method. The red curve represents the best fit to all three samples, and results in an unrealistically-high till density of 4.5 g/cm^3 (red curve), whereas the blue curve is only based on the two samples at greatest depth and results in a realistic till density of 1.3 g/cm^3. The black crosses represent the depths at which the two curves attain the average exposure of four boulders (group J, Fig. 4C, Table 1) embedded in the same moraine (this happens at 14 cm above and 55 cm below the current surface). (B) photograph of the till section with sample locations indicated at 20, 83 and 202 cm depths below the surface (yellow triangles in panel a). (For interpretation of the references to color in this figure legend, the reader is referred to the web version of this article.)

the four boulder exposure ages are closely clustered), and requires an unusually high till density of 4.5 g/cm^3. However, if only the two samples at greatest depth are used, both the surface concentration N_0 (8.86 $\times$ 10^5 atoms/g) and till density (1.3 g/cm^3) shift toward values in-line with expectations. Hence, the regression based on the bottom two samples yields more realistic results in terms of the till density required to fit the independent data provided by the boulder nuclide concentrations, and yields a surface nuclide concentration in much closer agreement with them. The apparently anomalously high radionuclide concentration of the top till section sample could be caused by inheritance from bedrock or sediment with prior exposure. Assuming the average boulder exposure ages approximately reflect the exposure age of the till profile, a target nuclide concentration of 9.97 $\times$ 10^5 atoms/g for the till profile surface is derived from the average boulder exposure age of 15.9 ka and a density of 1.3 g/cm^3. The projections for the predicted till surface nuclide concentrations are located at 14 cm above and 55 cm below the current till surface for the two scenarios (Fig. 6A).

Using the two samples at greatest depth, the predicted surface cosmogenic isotope concentration was converted to an exposure age (14.3 $\pm$ 1.2 ka) using the same method as for the boulder samples. This apparent age is younger than the apparent boulder ages (15.2 $\pm$ 1.4–17.1 $\pm$ 1.6 ka). This difference may reflect partial shielding of the moraine surface by boulders, postglacial erosion of the till surface, or may be apparent because all estimates are minimum estimates only. The disparity in age between the three samples from the till section indicate that the pebbles were derived from various sources and that care should be taken in interpreting till profile data.

6.4. Glacial history of the Shaluli Shan area

Three major glacial stages can be identified based on the ^{10}Be results: pre-gLGM glaciation(s) with moraine minimum ages ranging from 102.3 $\pm$ 10.0 to 183.6 $\pm$ 17.0 ka, gLGM glaciation at 21.6 $\pm$ 2.0 ka, and Late Glacial advances or standstills between 13.0 $\pm$ 1.2 and 17.1 $\pm$ 1.6 ka.

6.4.1. Pre-gLGM glaciation

Boulders from 9 moraines and 6 dispersed erratic groups sampled in the study area have ages ranging between 40.3 $\pm$ 3.7 and 183.6 $\pm$ 17.0 ka, and allow us to refine previous knowledge of the chronology of glaciations in the Shaluli Shan and the southeastern Tibetan Plateau (Fig. 5). Our ^{10}Be exposure age results include ages that are significantly older than previous TCN ages for glacial landforms in the Shaluli Shan and the southeastern Tibetan Plateau, and these are minimum estimates assuming zero erosion and, based on the erosion-correction analysis presented above, derived ages may underestimate depositional ages by 10%–230%. The older ages indicate at least one glaciation during MIS 6, or older. However, the large age scatter for moraines and dispersed boulders inhibit more definite conclusions regarding the presence of multiple glaciations. Following Heyman et al. (2011a) we take the oldest apparent age in each set of dates from a single location as the minimum age of glaciation/landform formation (Fig. 5B). Hence, the discussion below is based on the minimum age of glaciation inferred from boulder groups on moraines and groups of dispersed boulders.

The minimum age for our oldest group of moraines ranges from 102.3 $\pm$ 10.0 to 183.6 $\pm$ 17.0 ka. This group includes the Kuzhaori moraine complex, consisting of 5 ridges, from which four boulder groups were sampled (B–E). Boulder groups C, D, and E on the Kuzhaori moraine complex have overlapping ages at 85.7 $\pm$ 7.8–106.9 $\pm$ 9.6, 50.6 $\pm$ 4.6–117.2 $\pm$ 10.9, and 105.7 $\pm$ 9.3–123.8 $\pm$ 11.7 ka, respectively (Fig. 4A), while boulders on the most distal of these overlapping moraines (group B) show an age range of 121.3 $\pm$ 10.8 to 150.7 $\pm$ 14.2 ka. The isolated ridge remnants (group A), is truncated in its frontal section and, in combination with its apparent age range of almost 110 kyr (40.3 $\pm$ 3.7 and 149.2 $\pm$ 13.5 ka), this indicates that it perhaps formed during an earlier glacial advance than the glacial advance that formed the overlapping moraine complex. Groups C and E show an age range of about 20 kyr, while group D shows an age range of 67 kyr. Moraines with similar morphology and relative position occur abundantly around the Haizishan Plateau (Fu et al., 2013; Fig. 3A), Mt. Genie, Quer Shan, and in other alpine glacier areas. Age ranges of moraine boulder groups H, M, and P are consistent with the age ranges of the Kuzhaori moraines, indicating formation during the same glaciation. This dataset, together with the landform distribution map (Fu et al., 2012; Fig. 3A), indicates the presence of an extensive ice cap on the Haizishan Plateau with outlet glaciers that extended far down the surrounding valleys, and extensive valley glaciers or piedmont glaciers in high alpine areas during the glaciation much older than gLGM. Based on the moraine distribution and geomorphological observations in the field (Fu et al., 2013), it is clear that glacier- and/or moraine-dammed lakes formed in some of the valleys which, when they drained, may have eroded existing end moraines, leaving behind the isolated remnants that are visible today, for example the locations of groups G and F (Fig. 4B).

The oldest age in our data set, 183.6 ± 17.0 ka, is from a moraine boulder group in Nata (Group Q; Table 1, Fig. 4F). No glacial evidence was mapped or observed beyond the moraines in the Nata region. The Nata moraine complex is degraded and the occasional boulders that are scattered on the moraine ridge have surfaces that were similarly weathered as boulders that we observed on the moraine at Heranseba (Fig. 4G). The Nata moraine has the oldest glacial boulder exposure age so far on the southeastern Tibetan Plateau.

The nine oldest boulder exposure ages are likely correlated with MIS 6 or even older period (Fig. 5B). This is because the ages presented here are based on the Lal-Stone time-dependent nuclide production scheme (Lal, 1991; Stone, 2000) with zero erosion, and thus underestimates landform ages in the presence of erosion.

Although the Nata moraine has the oldest exposure age in our study, the isolated Kuzhaori ridge (group A in Fig. 4A), with minimum ages of 40.3 ± 3.7 and 149.2 ± 13.5 ka (Table 1), has previously been identified as belonging to the oldest glacial moraine sequence in southeastern Tibet (Zheng and Ma, 1995; Zhou et al., 2007; Xu et al., 2010). The ridge consists of red weathered sediments and the boulders that were sampled were standing low above the ridge surface adjacent to gullies. The field setting indicates active degradation and the apparent ages, therefore, again underestimate the true age of this moraine. Its location, its truncation, and its weathered sediments and gullied surface all support an interpretation that its formation happened during an older event than the neighboring Kuzhaori moraine complex (groups B–E).

Groups F and G in Sangdui (Fig. 4B), group I on the Haizishan Plateau (Fig. 4I), group L off the northern margin of the Haizishan Plateau (Fig. 4D), and group O on the Xinlong Plateau (Fig. 4E) consist of samples from dispersed boulders. The oldest age of each group ranges from 95.9 ± 8.7 ka (group G) to 156.0 ± 14.1 ka (group I), consistent with the oldest ages of moraine boulders (Fig. 5B). Group I on the Haizishan Plateau surface (Figs. 4C and 5A) also has the youngest age in the study area (8.1 ± 0.8) and therefore the largest range in this study. If all the youngest ages of the different groups clustered together, then that might be significant, but this seems not to be the case. So the youngest ages are perhaps without consequences for reconstructing glacial histories, but have some meaning as an indication of recent exposure, possibly due to fluvial erosion which evacuated till covers.

6.4.2. gLGM (MIS 2) glaciation

Because a major emphasis of our sampling campaign was on dating the oldest glaciation, only one moraine yielded ages that are closely clustered and correspond to MIS 2 (group N; 17.1 ± 1.6, 20.2 ± 1.8, and 21.6 ± 2.0 ka). These ages are consistent with ages derived by Graf et al. (2008) for moraines on the north and south sides of the Xinlong Plateau (Figs. 4E, 5A) and by Zhou et al. (2007) from Boduizangbu valley. Adopting other erosion-correction values or different production rate models does not alter these ages beyond MIS 2. Hence, we argue that this moraine was formed during gLGM. However, with only three ages, we couldn't exclude other possibilities and this may need further testing.

The gLGM moraine is a lateral moraine located in the valley that drains the northern margin of the Haizishan Plateau (Fig. 4D). It is furthermore situated adjacent to the proximal side of a moraine interpreted as having been formed during MIS 6 or previous period (group M) and there is no moraine indicating another glacial advance between these two events (Fig. 4D). This implies that in the Shaluli Shan there was a maximum glaciation during the gLGM, and that gLGM glaciers overrode and reworked deposits from potential glaciations since MIS 6. Based on moraine morphostratigraphy and relative position, moraines that we interpreted as gLGM were mapped in many other outlet glacier valleys or alpine glacier valleys, which are the intermediate sequence of moraines in Fig. 4. Outlet glaciers off the Haizishan Plateau were several kilometers long in valleys to the north and east during gLGM, whereas the ice margin only reached the plateau margin in the southwest, probably because of less accumulation during gLGM than pre-gLGM. MIS 2 moraines in large valleys in areas with former alpine glaciation extend locally more than 30 km from mountain centers, such as the inner moraines in Heranseba (Fig. 4G).

6.4.3. Late Glacial glaciation

The Late Glacial exposure ages only occur on two sinuous moraines on the Haizishan Plateau with ages of 12.9 ± 1.2 and 13.0 ± 1.2 ka for group K boulders and between 15.2 ± 1.4 and 17.1 ± 1.6 ka for group J boulders (Fig. 4C). Because the ages within each group are clustered closely, inheritance or modifications by post-depositional processes appear negligible complications. Together with a prominent but undated moraine ridge between these two moraines, they indicate that the Haizishan ice cap experienced three standstills or re-advances during retreat from its gLGM. Recessional moraine sequences similar to those just described are also found in northern and eastern valleys off the Haizishan Plateau (e.g., the innermost moraine in Fig. 4D), on the Xinlong Plateau, and in alpine glacial areas close to valley heads. Hence, the Haizishan Plateau was still covered by an ice cap limited to part of the plateau surface, and alpine areas had small glaciers during the Late Glacial. The Late Glacial ages of moraines on the Haizishan Plateau are concordant with previous TCN results of moraine boulders in the nearby Litang area (Schäfer et al., 2002), on the Xinlong Plateau (Graf et al., 2008), and in the Kangding area (Strasky et al., 2009). These widely distributed moraines with younger than gLGM ages indicate that the Late Glacial glaciation stage (about 17–13 ka) was of regional importance. In some large valleys, for example off the northern Haizishan Plateau margin (Fig. 4D) and in the Quer Shan (Fig. 1), moraines interpreted to have formed during the gLGM and the Late Glacial are kilometers apart, while in some small valleys or valleys with narrow headwaters, the glaciers did reach similar positions and moraines from different stages can be difficult to distinguish. For this reason, we may consider the possibility that the westernmost dated moraine on the western Haizishan Plateau surface (Fig. 4C) could represent a late stage of the gLGM advance, especially considering that no older moraine (belonging to gLGM or older) has been mapped beyond the dated moraine.

6.5. The Kuzhaori moraine complex and ^{10}Be-ESR age comparisons

^{10}Be exposure ages for the sampled three overlapping innermost moraines (C, D, E in Fig. 4A) provide statistically consistent minimum ages at 106.9 ± 9.6, 117.2 ± 10.9, and 123.8 ± 11.7 ka and an outer moraine has a minimum age of 150.7 ± 14.2 ka (B in Fig. 4A). ESR ages from the main moraine complex range from 16.2 to 134.2 ka, and Xu and Zhou (2009) conclude that glaciations therefore occurred at MIS 6, MIS 3, early MIS 2, and gLGM (Fig. 7).

The contrast between the ESR and ^{10}Be apparent exposure ages from individual ridges of the same moraine complex highlight the challenge of comparing results from these two techniques elsewhere. The ESR method is based on measurements of the amount of paramagnetic electrons generated by α-, β- and γ-radiation of

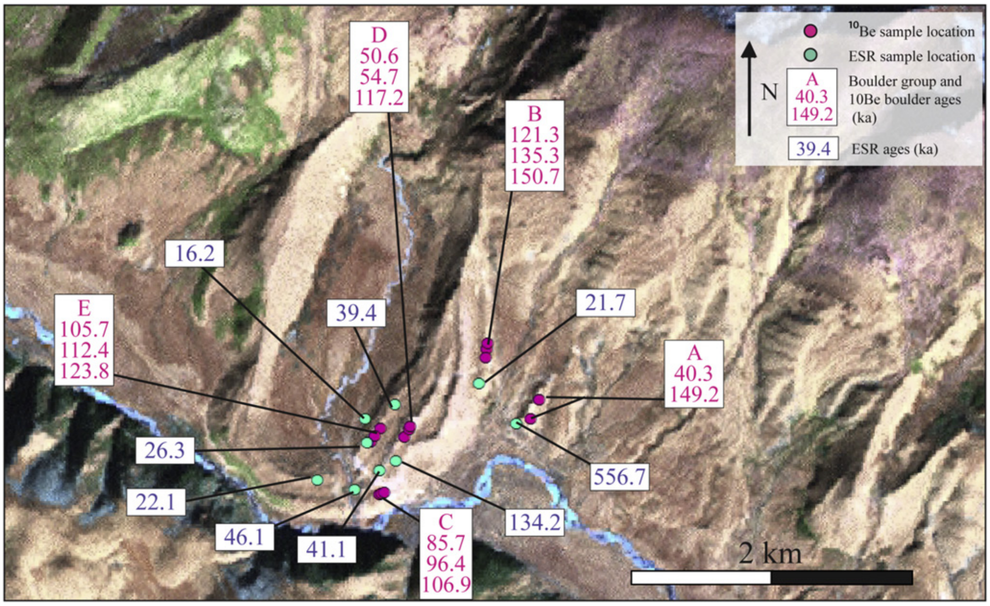

Fig. 7. Boulder ^{10}Be exposure locations (groups A–E) and ages (this study, purple dots, Table 1) and ESR ages (Xu and Zhou, 2009) of the Kuzhaori moraine complex and outermost moraine remnant. (For interpretation of the references to color in this figure legend, the reader is referred to the web version of this article.)

natural radio elements (e.g. U, Th, K) trapped in crystal defects as a measure of time since the ESR signal was last zeroed (Hennig and Grün, 1984; Grün, 1989). The application of ESR in dating glacial till is still largely experimental because it remains to be demonstrated that particle collision and abrasion during subglacial transport is sufficient to zero the signal from prior irradiation (Yi, 1997; Ye et al., 1998; Yi et al., 2007). If the sample is not completely zeroed, then inheritance causes an overestimate of the age of till deposition. TCN exposure age calculations also have a range of uncertainties (Gosse and Phillips, 2001) which complicate or inhibit the derivation of landform ages. However, despite such uncertainties, TCN exposure age dating has been widely applied for glacial chronologies because production rates are relatively-well known, the relative ubiquitous availability of sample material, and little effect on overall conclusion by methodological uncertainties (Balco, 2011). Because of the relative close clustering of the oldest ^{10}Be minimum exposure ages on the Kuzhaori complex of overlapping moraines, we conclude that they were formed before the gLGM, most likely during MIS 6, which is inconsistent with apparent age estimates from the ESR data by Xu and Zhou (2009).

The remnant ridge (location of group A in Fig. 7), within 1 km east of the Kuzhaori moraine complex, consists of deeply weathered sediments. Because the Kuzhaori moraine complex, however, lacks evidence of such weathering, the implication is that this period of extensive soil development and weathering occurred before MIS 6. Based on the deep weathering characteristics, previous studies (Zheng and Ma, 1995; Xu and Zhou, 2009) proposed that this feature represents the oldest and most extensive glaciation in the study area, which appears to be confirmed by the ESR age of 556.7 ka (Xu and Zhou, 2009). However, two exposure ages from this ridge occur at 40.3 ± 3.7 ka and 149.2 ± 13.5 ka, the latter of which seems to be concordant with the recalculated ^{10}Be exposure ages for another boulder (95.7–100.1 ka) by Wang et al. (2006) (Fig. 4A). Because these samples are from deeply weathered boulders standing quite low above the ridge surface, implying that these boulders were likely first exposed during ridge crest degradation, and subsequently experienced significant surface weathering, the resulting exposure ages clearly underestimate the depositional age of this ridge. So the age of the moraine using ^{10}Be exposure ages cannot be determined without more confident evidence of boulder erosion rate and ridge degradation history. The calculated minimum ^{10}Be surface exposure age by Wang et al. (2006), using two till profile samples, yielded 298.3 ka (recalculated 304.5 ka; Fig. 4A). This value further diversifies the situation because, in the absence of boulder erosion, the value is derived assuming zero ridge degradation and negligible plateau uplift. Whereas we know the former to be untrue, and therefore can only state apparent exposure ages as minimum ages only, the influence of plateau uplift on cosmogenic exposure age interpretations remains unsettled. The ability for deep weathering to occur on moraines at an altitude of 3890 m asl (with its cold and dry climate) has been questioned. Li et al. (1996) therefore argued that such weathering must have occurred at lower elevations (and under milder climatic conditions), and can therefore be used as evidence for a Pleistocene uplift of the Shaluli Shan. However, in a thermochronological study of deeply incised rivers on the southeastern Tibetan Plateau, Clark et al. (2005) argue that rapid uplift started during the Miocene, between 13 and 9 Ma. In addition, several geological and tectonic, stable isotope-based paleoaltimetry studies, and paleobotanical studies show that vast areas of the Plateau reached their current elevations before 8 Ma (Harrison et al., 1992; Coleman and Hodges, 1995; Fielding, 1996; Rowley et al., 2001; Tapponnier et al., 2001; Spicer et al., 2003; Cyr et al., 2005; Currie et al., 2005; Polissar et al., 2009; Saylor et al., 2009). Hence, without further evidence indicating a Pleistocene uplift of Shaluli Shan, we do not consider plateau uplift to have influenced derived cosmogenic nuclide concentrations of boulders on its moraines.

6.6. The gLGM across the Tibetan Plateau and Himalaya

Previous studies have shown that some regions of the Tibetan Plateau and Himalaya, like Tanggula Shan (Fig. 1), experienced much more extensive glacier advances during MIS 3 than during the gLGM (Owen et al., 2002, 2005; Finkel et al., 2003; Colgan et al., 2006). The northwestern region of the Tibetan Plateau, in contrast, has been characterized by extensive gLGM glacier advances (Phillips et al., 2000; Richards et al., 2000; Seong et al., 2007, 2009).

Based on such regional differences it has been argued that glacier advances in monsoon-dominated regions, such as the southeastern Tibetan Plateau, occurred out of synchrony with Northern Hemisphere climate change, but that glacier advances in regions influenced by the westerlies, such as the western Tibetan Plateau, occurred in synchrony with Northern Hemisphere climate change (Benn and Owen, 1998; Finkel et al., 2003; Owen et al., 2005, 2008).

Despite the fact that the precipitation of the Shaluli Shan today is dominated by monsoon circulation, we find evidence for extensive gLGM glaciation, including the growth of ice caps and extensive valleys glaciers, consistent with the record of Northern Hemisphere glaciation (Fig. 5B). The deglaciation chronology for the Shaluli Shan (17.1 ka) is consistent with the termination of the gLGM at about 17.5 ka (Schaefer et al., 2006). The timing of pre-gLGM glaciation (predating 102.3 ± 10.0–183.6 ± 17.0 ka) may also be consistent with the Northern Hemisphere record of glaciation although the evidence is not conclusive. In addition, there are no MIS 3/4 age moraines, whereas glaciers advanced in the Himalaya and Tanggula Shan during this time (Owen et al., 2002; Finkel et al., 2003; Colgan et al., 2006). Although it remains unclear why glaciers did grow large in the Shaluli Shan during MIS 2, it is, however, evident that while they did they also must have eroded MIS 3/4 moraines if they were present. Interestingly, ^{10}Be boulder ages from moraines in two valleys in the middle part of the Hengduan Mountains, 400 km west of the Shaluli Shan, were interpreted to have formed at MIS 2 and MIS 6 (Zhou et al., 2007). The apparently consistent timing of glacial advances in two locations within the Hengduan Mountains of the southeastern Tibetan Plateau, and at odds with expectations for monsoon-dominated precipitation regimes, calls into question our current understanding of regional differences in glacier response across the Himalayas and Tibetan Plateau and their paleoclimate significance.

7. Conclusions

Based on field investigation, geomorphological mapping and ^{10}Be exposure dating we examined the glacial history of Shaluli Shan and draw the following conclusions.

- Late Glacial, global LGM (gLGM) and pre-gLGM glaciations have been identified in the Shaluli Shan. Pre-gLGM glaciations are likely of MIS 6 age or older. There is evidence for at least one older glaciation, the deposits of which are deeply weathered.
- Dates from the Kuzhaori moraine complex with overlapping terminal moraines indicate deposition during MIS 6, or earlier, with minimum ages ranging from 102.3 ± 10.0–183.6 ± 17.0 ka. An independent study of the moraines by Xu and Zhou (2009) using ESR yielded glaciations occurring at gLGM, early MIS 2, MIS 3 and MIS 6. The contrast between the ESR and ^{10}Be apparent exposure ages from individual ridges of the same moraine complex highlight the challenge of comparing results from these two techniques elsewhere.
- The timing and extents of the glaciations on the southeastern Tibetan Plateau, an area dominated by monsoon precipitation, appear correlated to variations in Northern Hemispheric climate. These results reaffirm the need for a better understanding of the paleoclimate significance of regional differences in glacier response across the Himalayas and the Tibetan Plateau.

Acknowledgments

We thank J. Feng, B. Heyman, and E. Johansson for field assistance. We thank D. Granger for constructive remarks that improved the paper. We thank L. Owen and L.B. Xu for critical reviews. Funding for fieldwork and group workshops was provided by the Swedish Research Council/Swedish International Development Cooperation Agency (VR/SIDA) through their Swedish Research Links programme to Stroeven (No. 578 348-2004-5684 and 348-2007-6924). Partial funding for exposure dating was provided by the Swedish Society for Anthropology and Geography and The Royal Swedish Academy of Sciences to Fu, and by the Swedish Society for Anthropology and Geography, Carl Mannerfelts fond, and stiftelsen Längmanska kulturfonden to Heyman.

Appendix A. Supplementary material

Supplementary material related to this article can be found at http://dx.doi.org/10.1016/j.quascirev.2012.12.009.

References

Abramowski, U., Bergau, A., Seebach, D., Zech, R., Glaser, B., Sosin, P., Kubik, P.W., Zech, W., 2006. Pleistocene glaciations of Central Asia: results from ^{10}Be surface exposure ages of erratic boulders from the Pamir (Tajikistan), and the Alay–Turkestan range (Kyrgyzstan). Quaternary Science Reviews 25 (9–10), 1080–1096.

Applegate, P.J., Urban, N.M., Laab, B.J.C., Keller, K., Alley, R.B., 2010. Modeling the statistical distributions of cosmogenic exposure dates from moraines. Geoscientific Model Development 3 (1), 293–307. http://dx.doi.org/10.5194/gmd-3-293-2010.

Applegate, P.J., Urban, N.M., Keller, K., Lowell, T.V., Laabs, B.J.C., Kelly, M.A., Alley, R.B., 2012. Improved moraine age interpretations through explicit matching of geomorphic process models to cosmogenic nuclide measurements from single landforms. Quaternary Research 77 (2), 293–304. http://dx.doi.org/10.1016/j.yqres.2011.12.002.

Balco, G., 2011. Contributions and unrealized potential contributions of cosmogenic-nuclide exposure dating to glacier chronology, 1990–2010. Quaternary Science Reviews 30 (1–2), 3–27.

Balco, G., Stone, J.O., Lifton, N.A., Dunai, T.J., 2008. A complete and easily accessible means of calculating surface exposure ages or erosion rates from ^{10}Be and ^{26}Al measurements. Quaternary Geochronology 3 (3), 174–195. http://dx.doi.org/10.1016/j.quageo.2007.12.001.

Benn, D.I., Owen, L.A., 1998. The role of the Indian summer monsoon and the mid-latitude westerlies in Himalayan glaciation: review and speculative discussion. Journal of the Geological Society 155 (2), 353–363. http://dx.doi.org/10.1144/gsjgs.155.2.0353.

Bradley, R.S., 2001. Paleoclimatology: Reconstructing Climates of the Quaternary, second ed. Academic Press Limited, London, 211 pp.

Briner, J.P., Kaufman, D.S., Manley, W.F., Finkel, R.C., Caffee, M.W., 2005. Cosmogenic exposure dating of late Pleistocene moraine stabilization in Alaska. Geological Society of America Bulletin 117 (7–8), 1108–1120. http://dx.doi.org/10.1130/b25649.1.

Chmeleff, J., von Blanckenburg, F., Kossert, K., Jakob, D., 2010. Determination of the ^{10}Be half-life by multicollector ICP-MS and liquid scintillation counting. Nuclear Instruments and Methods in Physics Research Section B: Beam Interactions with Materials and Atoms 268 (2), 192–199.

Clark, M.K., House, M.A., Royden, L.H., Whipple, K.X., Burchfiel, B.C., Zhang, X., Tang, W., 2005. Late Cenozoic uplift of southeastern Tibet. Geology 33 (6), 525–528. http://dx.doi.org/10.1130/g21265.1.

Coleman, M., Hodges, K., 1995. Evidence for Tibetan plateau uplift before 14 Myr ago from a new minimum age for east-west extension. Nature 374 (6517), 49–52.

Colgan, P.M., Munroe, J.S., Zhou, S.Z., 2006. Cosmogenic radionuclide evidence for the limited extent of last glacial maximum glaciers in the Tanggula Shan of the central Tibetan Plateau. Quaternary Research 65 (2), 336–339. http://dx.doi.org/10.1016/j.yqres.2005.08.026.

Currie, B.S., Rowley, D.B., Tabor, N.J., 2005. Middle Miocene paleoaltimetry of southern Tibet: Implications for the role of mantle thickening and delamination in the Himalayan orogen. Geology 33 (3), 181–184.

Cyr, A.J., Curie, B.S., Rowley, D.B., 2005. Geochemical Evaluation of Fenghuoshan Group Lacustrine Carbonates, North-central Tibet: Implications for the Paleoaltimetry of the Eocene Tibetan Plateau, 113. University of Chicago Press, Chicago, 17 pp.

Delmas, M., Calvet, M., Gunnell, Y., 2009. Variability of Quaternary glacial erosion rates – a global perspective with special reference to the Eastern Pyrenees. Quaternary Science Reviews 28 (5–6), 484–498.

Derbyshire, E., Shi, Y., Li, J., Zheng, B., Li, S., Wang, J., 1991. Quaternary glaciation of Tibet: the geological evidence. Quaternary Science Reviews 10 (6), 485–510. http://dx.doi.org/10.1016/0277-3791(91)90042-S.

Desilets, D., Zreda, M., Prabu, T., 2006. Extended scaling factors for in situ cosmogenic nuclides: new measurements at low latitude. 246, 265–276.

Dortch, J.M., Owen, L.A., Caffee, M.W., Brease, P., 2010. Late Quaternary glaciation and equilibrium line altitude variations of the McKinley River region, central

Alaska Range. Boreas 39 (2), 233–246. http://dx.doi.org/10.1111/j.1502-3885.2009.00121.x.
Dunai, T., 2001. Influence of secular variation of the magnetic field on production rates of in situ produced cosmogenic nuclides. Earth and Planetary Science Letters 193, 197–212.
Fabel, D., Harbor, J., 1999. The use of in-situ produced cosmogenic radionuclides in glaciology and glacial geomorphology. Annals of Glaciology 28 (1), 103–110. http://dx.doi.org/10.3189/172756499781821968.
Fielding, E.J., 1996. Tibet uplift and erosion. Tectonophysics 260 (1–3), 55–84.
Finkel, R.C., Owen, L.A., Barnard, P.L., Caffee, M.W., 2003. Beryllium-10 dating of Mount Everest moraines indicates a strong monsoon influence and glacial synchroneity throughout the Himalaya. Geology 31 (6), 561–564. http://dx.doi.org/10.1130/0091-7613(2003)031<0561:bdomem>2.0.co;2.
Fu, P., Heyman, J., Hättestrand, C., Stroeven, A.P., Harbor, J., 2012. Glacial geomorphology of the Shaluli Shan, southeastern Tibetan Plateau. Journal of Maps 8 (1), 48–55.
Fu, P., Harbor, J.M., Stroeven, A.P., Hättestrand, C., Heyman, J., Zhou, L., 2013. Glacial geomorphology and paleoglaciation patterns in Shaluli Shan, the southeastern Tibetan Plateau – evidence for polythermal ice cap glaciation. Geomorphology 182, 66–78. http://dx.doi.org/10.1016/j.geomorph.2012.10.030.
Gosse, J.C., Phillips, F.M., 2001. Terrestrial in situ cosmogenic nuclides: theory and application. Quaternary Science Reviews 20 (14), 1475–1560. http://dx.doi.org/10.1016/s0277-3791(00)00171-2.
Graf, A.A., Strasky, S., Zhao, Z.Z., Akçar, N., Ivy-Ochs, S., Kubik, P.W., Christl, M., Kasper, H.U., Wieler, R., Schlüchter, C., 2008. Glacier extension on the eastern Tibetan Plateau in response to MIS 2 cooling, with a contribution to ^{10}Be and ^{21}Ne methodology. In: Strasky, S. (Ed.), Glacial response to global climate changes: cosmogenic nuclide chronologies from high and low latitudes. PhD thesis, ETH Zürich. University of Bern, Bern, pp. 77–110.
Grün, R., 1989. Electron spin resonance (ESR) dating. Quaternary International 1, 65–109.
Hallet, B., Putkonen, J., 1994. Surface dating of dynamic landforms: young boulders on aging moraines. Science 265 (5174), 937–940. http://dx.doi.org/10.1126/science.265.5174.937.
Hallet, B., Hunter, L., Bogen, J., 1996. Rates of erosion and sediment evacuation by glaciers: a review of field data and their implications. Global and Planetary Change 12 (1–4), 213–235. http://dx.doi.org/10.1016/0921-8181(95)00021-6.
Harris, N., 2006. The elevation history of the Tibetan Plateau and its implications for the Asian monsoon. Palaeogeography, Palaeoclimatology, Palaeoecology 241 (1), 4–15. http://dx.doi.org/10.1016/j.palaeo.2006.07.009.
Harrison, T.M., Copeland, P., Kidd, W.S.F., Yin, A., 1992. Raising Tibet. Science in China Series B-Chemistry 255 (5052), 1663–1670.
Heinrich, H., 1988. Origin and consequences of cyclic ice rafting in the Northeast Atlantic Ocean during the past 130,000 years. Quaternary Research 29 (2), 142–152. http://dx.doi.org/10.1016/0033-5894(88)90057-9.
Hennig, G.J., Grün, R., 1984. ESR dating in Quaternary geology. Quaternary Science Reviews 2, 157–238.
Heyman, J., Stroeven, A.P., Harbor, J.M., Caffee, M.W., 2011a. Too young or too old: evaluating cosmogenic exposure dating based on an analysis of compiled boulder exposure ages. Earth and Planetary Science Letters 302 (1–2), 71–80. http://dx.doi.org/10.1016/j.epsl.2010.11.040.
Heyman, J., Stroeven, A.P., Caffee, M.W., Hättestrand, C., Harbor, J., Li, Y.K., Alexanderson, H., Zhou, L.P., Hubbard, A., 2011b. Palaeoglaciology of Bayan Har Shan, NE Tibetan Plateau: exposure ages reveal a missing LGM expansion. Quaternary Science Reviews 30 (15–16), 1988–2001. http://dx.doi.org/10.1016/j.quascirev.2011.05.002.
Ivy-Ochs, S., Kerschner, H., Kubik, P.W., Schlüchter, C., 2006. Glacier response in the European Alps to Heinrich Event 1 cooling: the Gschnitz stadial. Journal of Quaternary Science 21 (2), 115–130.
Jarvis, A., Reuter, H.I., Nelson, A., Guevara, E., 2008. Hole-filled Seamless SRTM Data V4. International Centre for Tropical Agriculture. Available from: http://srtm.csi.cgiar.org (retrieved in August 2009).
Kohl, C.P., Nishiizumi, K., 1992. Chemical isolation of quartz for measurement of in-situ -produced cosmogenic nuclides. Geochimica et Cosmochimica Acta 56 (9), 3583–3587. http://dx.doi.org/10.1016/0016-7037(92)90401-4.
Kong, P., Fink, D., Na, C., Huang, F., 2009. Late Quaternary glaciation of the Tianshan, Central Asia, using cosmogenic ^{10}Be surface exposure dating. Quaternary Research 72 (2), 229–233. http://dx.doi.org/10.1016/j.yqres.2009.06.002.
Koppes, M., Gillespie, A.R., Burke, R.M., Thompson, S.C., Stone, J., 2008. Late Quaternary glaciation in the Kyrgyz Tien Shan. Quaternary Science Reviews 27 (7–8), 846–866. http://dx.doi.org/10.1016/j.quascirev.2008.01.009.
Korschinek, G., Bergmaier, A., Faestermann, T., Gerstmann, U.C., Knie, K., Rugel, G., Wallner, A., Dillmann, I., Dollinger, G., von Gostomski, C.L., Kossert, K., Maiti, M., Poutivtsev, M., Remmert, A., 2010. A new value for the half-life of ^{10}Be by Heavy-Ion Elastic Recoil Detection and liquid scintillation counting. Nuclear Instruments and Methods in Physics Research Section B: Beam Interactions with Materials and Atoms 268 (2), 187–191. http://dx.doi.org/10.1016/j.nimb.2009.09.020.
Lal, D., 1991. Cosmic ray labeling of erosion surfaces: in situ nuclide production rates and erosion models. Earth and Planetary Science Letters 104 (2–4), 424–439. http://dx.doi.org/10.1016/0012-821x(91)90220-c.
Lehmkuhl, F., Owen, L.A., Derbyshire, E., 1998. Late Quaternary glacial history of northeast Tibet. Quaternary Proceedings 6, 121–142.
Li, B.Y., Li, J.J., Cui, Z.J., Zheng, B.X., Zhang, Q.S., Wang, F.B., Zhou, S.Z., Shi, Z.H., Jiao, K.Q., Kang, J.C., 1991. Quaternary Glacial Distribution Map of Qinghai-Xizang (Tibet) Plateau. Science Press, Beijing. Mapscale 1:3,000,000 (in Chinese).
Li, J.J., Feng, Z., Zhou, S.Z., 1996. Quaternary glacial remnants in Hengduan Shan. In: Li, J.J. (Ed.), Glaciers in Hengduan Shan. Science Press, Beijing, pp. 157–173 (in Chinese).
Lifton, N., Bieber, J., Clem, J., Duldig, M., Evenson, P., Humble, J., Pyle, R., 2005. Addressing solar modulation and long-term uncertainties in scaling secondary cosmic rays for in situ cosmogenic nuclide applications. Earth and Planetary Science Letters 239, 140–161.
Liu, G., Zhang, X., Cui, Z., Wu, Y., Ju, Y., 2006. A review of glacial sequences of the Kunlun Pass, northern Tibetan Plateau. Quaternary International 154–155, 63–72. http://dx.doi.org/10.1016/j.quaint.2006.02.004.
Molnar, P., England, P., 1990. Late cenozoic uplift of mountain-ranges and global climate change: chicken or egg? Nature 346 (6279), 29–34.
Montgomery, D.R., 2002. Valley formation by fluvial and glacial erosion. Geology 30 (11), 1047–1050.
Nelder, J.A., Mead, R., 1965. A simplex method for function minimization. Computer Journal 7, 308–313.
Nishiizumi, K., Imamura, M., Caffee, M.W., Southon, J.R., Finkel, R.C., McAninch, J., 2007. Absolute calibration of ^{10}Be AMS standards. Nuclear Instruments and Methods in Physics Research Section B: Beam Interactions with Materials and Atoms 258 (2), 403–413. http://dx.doi.org/10.1016/j.nimb.2007.01.297.
Nishiizumi, K., Winterer, E.L., Kohl, C.P., Klein, J., Middleton, R., Lal, D., Arnold, J.R., 1989. Cosmic ray production rates of ^{10}Be and ^{26}Al in quartz from glacially polished rocks. Journal of Geophysical Research 94 (B12), 17907–17915. http://dx.doi.org/10.1029/JB094iB12p17907.
Owen, L.A., 2009. Latest Pleistocene and Holocene glacier fluctuations in the Himalaya and Tibet. Quaternary Science Reviews 28 (21–22), 2150–2164. http://dx.doi.org/10.1016/j.quascirev.2008.10.020.
Owen, L.A., Finkel, R.C., Caffee, M.W., Gualtieri, L., 2002. Timing of multiple late Quaternary glaciations in the Hunza Valley, Karakoram Mountains, northern Pakistan: defined by cosmogenic radionuclide dating of moraines. Geological Society of America Bulletin 114 (5), 593–604. http://dx.doi.org/10.1130/0016-7606(2002)114<0593:TOMLQG>2.0.CO;2.
Owen, L.A., Caffee, M.W., Finkel, R.C., Seong, Y.B., 2008. Quaternary glaciation of the Himalayan–Tibetan orogen. Journal of Quaternary Science 23 (6–7), 513–531. http://dx.doi.org/10.1002/jqs.1203.
Owen, L.A., Caffee, M.W., Bovard, K.R., Finkel, R.C., Sharma, M.C., 2006. Terrestrial cosmogenic nuclide surface exposure dating of the oldest glacial successions in the Himalayan orogen: Ladakh Range, northern India. Geological Society of America Bulletin 118 (3–4), 383–392. http://dx.doi.org/10.1130/b25750.1.
Owen, L.A., Finkel, R.C., Ma, H., Spencer, J.Q., Derbyshire, E., Barnard, P.L., Caffee, M.W., 2003. Timing and style of Late Quaternary glaciation in northeastern Tibet. Geological Society of America Bulletin 115 (11), 1356–1364. http://dx.doi.org/10.1130/b25314.1.
Owen, L.A., Finkel, R.C., Barnard, P.L., Ma, H.Z., Asahi, K., Caffee, M.W., Derbyshire, E., 2005. Climatic and topographic controls on the style and timing of Late Quaternary glaciation throughout Tibet and the Himalaya defined by ^{10}Be cosmogenic radionuclide surface exposure dating. Quaternary Science Reviews 24 (12–13), 1391–1411.
Owen, L.A., Thackray, G., Anderson, R.S., Briner, J., Kaufman, D., Roe, G., Pfeffer, W., Yi, C., 2009a. Integrated research on mountain glaciers: current status, priorities and future prospects. Geomorphology 103 (2), 158–171. http://dx.doi.org/10.1016/j.geomorph.2008.04.019.
Owen, L.A., Robinson, R., Benn, D.I., Finkel, R.C., Davis, N.K., Yi, C., Putkonen, J., Li, D., Murray, A.S., 2009b. Quaternary glaciation of Mount Everest. Quaternary Science Reviews 28 (15–16), 1412–1433. http://dx.doi.org/10.1016/j.quascirev.2009.02.010.
Phillips, W.M., Sloan, V.F., Shroder, J.F., Sharma, P., Clarke, M.L., Rendell, H.M., 2000. Asynchronous glaciation at Nanga Parbat, northwestern Himalaya Mountains, Pakistan. Geology 28 (5), 431–434.
Polissar, P.J., Freeman, K.H., Rowley, D.B., McInerney, F.A., Currie, B.S., 2009. Paleoaltimetry of the Tibetan Plateau from D/H ratios of lipid biomarkers. Earth and Planetary Science Letters 287 (1–2), 64–76. http://dx.doi.org/10.1016/j.epsl.2009.07.037.
Putkonen, J., Swanson, T., 2003. Accuracy of cosmogenic ages for moraines. Quaternary Research 59 (2), 255–261. http://dx.doi.org/10.1016/s0033-5894(03)00006-1.
Putkonen, J., O'Neal, M., 2006. Degradation of unconsolidated Quaternary landforms in the western North America. Geomorphology 75 (3–4), 408–419. http://dx.doi.org/10.1016/j.geomorph.2005.07.024.
Putkonen, J., Connolly, J., Orloff, T., 2008. Landscape evolution degrades the geologic signature of past glaciations. Geomorphology 97 (1–2), 208–217. http://dx.doi.org/10.1016/j.geomorph.2007.02.043.
Raymo, M.E., Ruddiman, W.F., 1992. Tectonic forcing of late Cenozoic climate. Nature 359 (6391), 117–122.
Richards, B.W.M., 2000. Luminescence dating of Quaternary sediments in the Himalaya and High Asia: a practical guide to its use and limitations for constraining the timing of glaciation. Quaternary International 65–66, 49–61. http://dx.doi.org/10.1016/s1040-6182(99)00036-1.
Richards, B.W.M., Owen, L.A., Rhodes, E.J., 2000. Timing of Late Quaternary glaciations in the Himalayas of northern Pakistan. Journal of Quaternary Science 15, 283–297. http://dx.doi.org/10.1002/(SICI)1099-1417(200003)15:3<283::AID-JQS525>3.0.CO;2-X.

Rowley, D.B., Pierrehumbert, R.T., Currie, B.S., 2001. A new approach to stable isotope-based paleoaltimetry: implications for paleoaltimetry and paleohypsometry of the High Himalaya since the Late Miocene. Earth and Planetary Science Letters 188 (1–2), 253–268. http://dx.doi.org/10.1016/s0012-821x(01)00324-7.

Saylor, J.E., Quade, J., Dellman, D.L., DeCelles, P.G., Kapp, P.A., Ding, L., 2009. The late Miocene through present paleoelevation history of southwestern Tibet. American Journal of Science 309 (1), 1–42. http://dx.doi.org/10.2475/01.2009.01.

Schaefer, J.M., Denton, G.H., Barrell, D.J.A., Ivy-Ochs, S., Kubik, P.W., Andersen, B.G., Phillips, F.M., Lowell, T.V., Schlüchter, C., 2006. Near-synchronous interhemispheric Termination of the Last Glacial Maximum in mid-latitudes. Science 312 (5779), 1510–1513. http://dx.doi.org/10.1126/science.1122872.

Schäfer, J.M., Tschudi, S., Zhao, Z., Wu, X., Ivy-Ochs, S., Wieler, R., Baur, H., Kubik, P.W., Schlüchter, C., 2002. The limited influence of glaciations in Tibet on global climate over the past 170000 yr. Earth and Planetary Science Letters 194 (3–4), 287–297.

Seong, Y.B., Owen, L.A., Yi, C., Finkel, R.C., 2009. Quaternary glaciation of Muztag Ata and Kongur Shan: evidence for glacier response to rapid climate changes throughout the Late Glacial and Holocene in westernmost Tibet. Geological Society of America Bulletin 121 (3–4), 348–365. http://dx.doi.org/10.1130/b26339.1.

Seong, Y.B., Owen, L.A., Bishop, M.P., Bush, A., Clendon, P., Copland, L., Finkel, R., Kamp, U., Shroder Jr., J.F., 2007. Quaternary glacial history of the Central Karakoram. Quaternary Science Reviews 26 (25–28), 3384–3405. http://dx.doi.org/10.1016/j.quascirev.2007.09.015.

Shi, Y.F., 2002. Characteristics of late Quaternary monsoonal glaciation on the Tibetan Plateau and in East Asia. Quaternary International 97/98, 79–91.

Shi, Y.F., Zheng, B.X., Su, X., 2006. Quaternary glacier, glaciations and interglacial oscillations and environmental change. In: Shi, Y.F., Cui, Z.J., Su, Z. (Eds.), The Quaternary Glaciations and Environmental Variations in China. Hebei Science and Technology Publishing House, pp. 43–45.

Shi, Y.F., Ren, B., Wang, J., Derbyshire, E., 1986. Quaternary glaciation in China. Quaternary Science Reviews 5, 503–507.

Spicer, R.A., Harris, N.B.W., Widdowson, M., Herman, A.B., Guo, S., Valdes, P.J., Wolfe, J.A., Kelley, S.P., 2003. Constant elevation of southern Tibet over the past 15 million years. Nature 421 (6923), 622–624. http://dx.doi.org/10.1038/nature01356.

Stone, J.O., 2000. Air pressure and cosmogenic isotope production. Journal of Geophysical Research 105 (B10), 23753–23759. http://dx.doi.org/10.1029/2000jb900181.

Strasky, S., Graf, A.A., Zhao, Z., Kubik, P.W., Baur, H., Schlüchter, C., Wieler, R., 2009. Late Glacial ice advances in southeast Tibet. Journal of Asian Earth Sciences 34 (3), 458–465. http://dx.doi.org/10.1016/j.jseaes.2008.07.008.

Tapponnier, P., Zhiqin, X., Roger, F., Meyer, B., Arnaud, N., Wittlinger, G., Jingsui, Y., 2001. Oblique stepwise rise and growth of the Tibet Plateau. Science 294 (5547), 1671–1677. http://dx.doi.org/10.1126/science.105978.

Wang, J., Raisbeck, G., Xu, X., Yiou, F., Bai, S., 2006. In situ cosmogenic ^{10}Be dating of the Quaternary glaciations in the southern Shaluli Mountain on the Southeastern Tibetan Plateau. Science in China Series D: Earth Sciences 49 (12), 1291–1298.

Xu, L.B., Zhou, S.Z., 2009. Quaternary glaciations recorded by glacial and fluvial landforms in the Shaluli Mountains, Southeastern Tibetan Plateau. Geomorphology 103, 268–275.

Xu, L.B., Ou, X.J., Lai, Z.P., Zhou, S.Z., Wang, J., Fu, Y.C., 2010. Timing and style of Late Pleistocene glaciation in the Queer Shan, northern Hengduan Mountains in the eastern Tibetan Plateau. Journal of Quaternary Science 25 (6), 957–966. http://dx.doi.org/10.1002/jqs.1379.

Ye, Y., Diao, S., He, J., Gao, J., Lei, X., 1998. ESR dating studies of Paleo-debris-flows deposition Dongchuan, Yunnan Province, China. Quaternary Geochronology 17, 1073–1076.

Yi, C., Zhu, Z., Wei, L., Cui, Z., Zheng, B., Shi, Y., 2007. Advances in numerical dating of Quaternary glaciations in China. Zeitschrift für Geomorphologie. Supplementary Issues 51 (2), 153–175. http://dx.doi.org/10.1127/0372-8854/2007/0051s2-0153.

Yi, C.L., 1997. Subglacial comminution in till – evidence from microfabric studies and grain size distributions. Journal of Glaciology 43 (145), 473–479.

Zheng, B.X., 2000. Quaternary glaciation and glacier evolution in the Yulong Mount, Yunan. Journal of Glaciology and Geocryology 22 (1), 54–61 (in Chinese, English abstract).

Zheng, B.X., 2001. Study on the Quaternary glaciation and the formation of the Moxi platform in the east slopes of the Mount Gongga. Journal of Glaciology and Geocryology 23 (3), 283–291 (in Chinese, English abstract).

Zheng, B.X., 2006. Quaternary glaciations in the Hengduan Mountains. In: Shi, Y.F., Cui, Z.J., Su, Z. (Eds.), The Quaternary Glaciations and Environmental Variations in China. Hebei Science and Technology Publishing House, pp. 407–441 (in Chinese).

Zheng, B.X., Ma, Q.H., 1995. A study on the geomorphological characteristics and glaciations in Paleo-Daocheng Ice Cap, western Sichuan. Journal of Glaciology and Geocryology 17, 23–32 (in Chinese, English abstract).

Zheng, B.X., Wang, S., 1996. A Study on the Paleo-glaciation and Paleo environment in the Source Area of the Yellow River. Journal of Glaciology and Geocryology 18 (3), 210–218 (in Chinese, English abstract).

Zheng, B.X., Rutter, N., 1998. On the problem of Quaternary glaciations, and the extent and patterns of Pleistocene ice cover in the Qinghai–Xizang (Tibet) Plateau. Quaternary International 45-46, 109–122.

Zheng, B.X., Xu, Q.Q., Shen, Y.P., 2002. The relationship between climate change and Quaternary glacial cycles on the Qinghai-Tibetan Plateau: review and speculation. Quaternary International 97-98, 93–101.

Zhou, S.Z., Xu, L.B., Colgan, P.M., Mickelson, D.M., Wang, X.L., Wang, J., Zhong, W., 2007. Cosmogenic ^{10}Be dating of Guxiang and Baiyu glaciations. Chinese Science Bulletin 52, 1387–1393. http://dx.doi.org/10.1007/s11434-007-0208-y.